Springer

Acta Mechanica Sinica

CrossMark click for updates

•INVITED REVIEW•

Acta Mech. Sin., Vol. 38, 121449 (2022)
https://doi.org/10.1007/s10409-022-09022-x

Failure behavior and criteria of metallic glasses

Yan Chen[1,2], and Lanhong Dai[1,2*]

[1] State Key Laboratory of Nonlinear Mechanics, Institute of Mechanics, Chinese Academy of Sciences, Beijing 100190, China;
[2] School of Engineering Science, University of Chinese Academy of Sciences, Beijing 101408, China

Received September 8, 2021; accepted December 2, 2021; published online February 23, 2022

Metallic glasses (MGs) constitute an emerging class of advanced structural materials due to their excellent mechanical properties. However, brittle failure at room temperature and the resultant complicated fracture behavior greatly limit their wide engineering applications. Over the past decades, the deformation and fracture in ductile or brittle mode referring to material compositions, load conditions, sample size, etc., have been widely studied, and significant progress has been made in understanding the failure behavior of MGs. Micromechanisms of fracture have been revealed involving shear banding, cavitation and the nature of the crack tip field. The ductile-to-brittle transition and inherent governing parameters have been found. To well describe and predict the failure behavior of MGs, failure criteria for ductile and brittle MGs have been established empirically or based on atomic interactions. In this paper, we provide a detailed review of the above advances and identify outstanding issues in the failure of MGs that need to be further clarified.

Metallic glasses, Failure behavior, Shear band, Cavitation, Failure criteria

Citation: Y. Chen, and L. Dai, Failure behavior and criteria of metallic glasses, Acta Mech. Sin. **38**, 121449 (2022), https://doi.org/10.1007/s10409-022-09022-x

1. Introduction

In solid-state science, one of the fundamental and most fascinating themes is the contrasting states of order and disorder. Materials in a disordered state have no long-range structural order and present quite a different deformation mechanism from crystalline solids. Instead of the dislocation mechanism, localized shear-driven rearrangements of atoms or molecules accommodate plastic deformation in disordered materials [1-3]. The mysteries within the disordered structure and the resultant deformation behavior have aroused great interest from researchers, but numerous problems remain elusive [4-8]. Metallic glasses (MGs) are new disordered materials with extremely high strengths but poor room-temperature ductility. Their limited plastic straining under tension impedes their wide application as advanced structural materials. In recent decades, substantial research efforts have been paid to the deformation and failure behavior of MGs, which is one of the most fundamental problems of these materials and has led to great progress in understanding their underlying physics [9-22].

Attributed to their short-range ordered structures, MGs exhibit a number of fundamental and unique mechanical behavior traits [11,23-26], such as obvious pressure sensitivity in yielding, shear dilatancy during deformation, and multiple failure modes. MGs may fail in ductile or brittle mode by necking [27], shear banding [12,28-31], or cavitation [15,32-34]. Combining experimental and computational studies, researchers have attempted to clarify the deformation and failure behavior at the macroscale, such as multiple fracture modes and tension-compression asymmetry, and at the microscale, i.e., flow unit, microdeformation modes, and fracture morphologies [11,12,21,35]. Some basic understandings have been received. The two fundamental unit processes in MGs are regarded to be shear transformation zones (STZs) [2,3] and tension transformation zones (TTZs) [15,36]. The origin of shear band formation is attributed to a thermomechanical coupling mechanism [28,37]. The shear band propagates in a simultaneous mode due to a shear

*Corresponding author. E-mail address: lhdai@lnm.imech.ac.cn (Lanhong Dai)
Executive Editor: Xiaoding Wei

displacement jump mechanism [38-41] or in a progressive mode analogous to crack propagation and induces cracking [29,42-45]. The plastic zone, which is a critical region ahead of the crack tip, governs the formation and propagation of shear bands or cracks, which construct a bridge between microdeformation and the overall failure behavior [19,46-49]. The inherent correlations of the macroductility or toughness with material parameters and atomic structure have been uncovered [14,50-52]. By taking the unique traits of fracture behavior into account, failure criteria were developed that comprehensively describe tensile or both tensile and compressive failure phenomena in MGs [14,52-54]. In this review, we focus on the failure behavior and criteria of MGs, including the related advances, and several critical issues need to be further clarified.

2. Ductile or brittle failure behavior

Initiated from the onset of irreversible deformation, the failure of the material covers the whole process from yielding to final fracture. Failure modes can be generally classified as ductile or brittle, which are determined by the extent of plastic deformation. Generally, fracture ensues immediately after yielding with little plasticity in brittle failure, while apparent plastic deformation is displayed before final fracture in ductile mode. MGs lack strain hardening and intrinsic crack propagation barriers, such as grain boundaries in crystalline metals and alloys, but can dissipate plastic energy by localized shear bands, in contrast to oxide crystal glasses [12]. Their fracture ability is normally intermediate between traditional brittle and ductile materials. A wide range of toughness from ~1 MPa $m^{1/2}$ to ~100 MPa $m^{1/2}$ was displayed in MGs depending on their components; MGs can be very brittle with a mode I fracture toughness K_{Ic} similar to silicate glasses and ceramics, while MGs can behave very toughly with K_{IC} akin to high toughness crystalline metals [17,50,55,56]. Such complexities in the deformation and failure phenomena of MGs are exhibited at both the macro- and microscales.

The ductile or brittle behavior presented by MGs is found to depend on a number of factors, such as alloy composition, cooling rate, structural relaxation, loading state, and sample size [27,29,51,57-61]. Under uniaxial tensile conditions, most monolithic MGs will fracture catastrophically with almost zero macroscopic plasticity at room temperature, with a few exceptions reported in nanoscale size samples [27] or some MGs with low *Tg*. In contrast, under uniaxial compression, limited and even large plasticity can be found in MGs [58,62,63]. These show an obvious tension-compression asymmetry. In addition to this plasticity/ductility difference, the perplexing failure asymmetry between tension and compression observed in MGs is also manifested by the failure mode and strength. Under tensile loading, shear failure or normal tensile fracture (quasi-cleavage) are two typical modes, while under compression, MGs fail by shear or splitting (Table 1). The shear plane of traditional crystalline metals is usually along the direction of the maximum shear stress, which is 45° with respect to the loading axis. MGs fail along the plane at angle $45° < \theta^{T} \leq 90°$ under tension and $0° < \theta^{C} \leq 45°$ under compression (Table 1). This implies that in addition to the deviatoric stresses, pressure or normal stress also plays a critical role in the failure of MGs [23,64-66]. As observed from numerous experimental investigations, the failure strength of MGs in uniaxial tension (σ^{T}) is usually smaller than that in uniaxial compression (σ^{C}) (Table 1), which is called the strength-differential (S-D) effect [67,68]. Several reasons have been found to induce this effect, such as nonlinear interactions between dislocations or interstitial solute atoms [69] or shear-caused dilatation [70]. It is believed that the S-D effect should be taken into account for a full description of failure behaviors in MGs.

The fracture toughness or plasticity of MGs, closely related to shear banding and crack branching around the crack tip, is accompanied by different characteristic fracture morphologies [17-19,46,50,96-100]. The ductile failure in MGs is generally controlled by strain [47] and may lead to several typical fracture patterns, including microscale cells, river-like vein patterns, or dimples [13,15,97,101-103]. The plastic zone in front of the crack tip plays a decisive role in the resultant fracture behavior. The Taylor instability process of a fluid meniscus was found to be a reason for these patterns [15,97]. In contrast, crack initiation in brittle MGs starts from cavity nucleation ahead of the crack tip and is usually under the control of stress [18]. Whether brittle fracture via cavitation occurs in MGs was reported to depend on the competition between the cavitation stress and the hydrostatic stress ahead of the crack tip [32,34]. Relative smooth fracture surfaces with nanoscale corrugations or featureless mirror zones are usually displayed in brittle fracture due to a local cleavage mechanism [15,104-107]. A random creation of cavities or voids at the microscale was revealed to lead to quasi-brittle corrugation patterns [106,107]. In very brittle MGs, the local softening mechanism still holds true. Xi et al. [97] reported the microductile fracture pattern, i.e., dimple structures in Mg-based MGs, and presented that fracture toughness is clearly correlated with plastic zone size for MGs. This implies that a local softening mechanism might occur along with the fracture of both brittle and ductile MGs but at different length scales.

3. Failure mechanisms

Ductile or brittle failure behavior in MGs highly depends on three basic microdeformation modes, namely, shear banding,

Table 1 Failure strengths and angles of MGs in tension and compression [14]

Composites	Failure strengths		Failure angles		Ref.
	σ^T (GPa)	σ^C (GPa)	θ^T (°)	θ^C (°)	
$Pd_{77.5}Cu_6Si_{16.5}$	1.44	1.51	50	45	[71]
$Pd_{78}Cu_6Si_{16}$	1.45	1.54	55	45	[72]
$Pd_{40}Ni_{40}P_{20}$	1.46	1.78	50	41.9	[73]
	1.6	1.74	56	42	[74,75]
$Zr_{40.1}Ti_{12}Ni_{9.3}Cu_{12.2}Be_{26.4}$	1.98	2.0	51.6	40.8	[76]
$Zr_{41.2}Ti_{13.8}Ni_{10}Cu_{12.5}Be_{22.5}$	1.8	2.0	55	44	[15]
	1.8	1.95	56	42	[77]
	1.89	1.9	–	–	[78]
$Zr_{52.5}Ni_{14.6}Al_{10}Cu_{17.9}Ti_5$	1.65	1.88	54	44	[79]
	1.66	1.82	60	42.5	[80]
	1.66	1.76	56	42	[81]
$Zr_{55}Al_{10}Cu_{30}Ni_5$	1.53	1.77	53	41	[82]
	1.6	1.8	–	–	[83]
	1.51	1.82	–	–	[84]
$Zr_{56.2}Ti_{13.8}Nb_{5.0}Ni_{5.6}Cu_{6.9}Be_{12.5}$	1.487	1.669	59	45	[85]
$Zr_{57}Cu_{15.4}Ni_{12.6}Al_{10}Nb_5$	1.2	1.8	–	–	[86]
$Zr_{59}Cu_{20}Al_{10}Ni_8Ti_3$	1.58	1.69	54	43	[87]
$Zr_{60}Al_{10}Cu_{20}Pd_{10}$	1.68	1.88	55	45	[88]
$Zr_{60}Al_{10}Cu_{25}Ni_5$	1.63	1.76	–	–	[82]
$Co_{80}Nb_{14}B_6$	2.88	3.47	–	–	[73]
$Cu_{60}Zr_{30}Ti_{10}$	2.0	2.15	–	–	[89]
$Cu_{60}Hf_{25}Ti_{15}$	2.13	2.16	–	–	[89]
$Pd_{80}Si_{20}$	1.33	–	90	–	[90]
$(Al_{84}Y_9Ni_5Co_2)_{0.95}Sn_5$	–	–	90		[91]
$La_{62}Al_{14}(Cu,Ni)_{24}$	0.55	0.56	90	40-45	[92]
$Zr_{52.5}Ni_{14.6}Al_{10}Cu_{17.9}Ti_5$	–	–	90		[93]
$Zr_{59}Cu_{20}Al_{10}Ni_8Ti_3$	–	–	90		[93]
$Zr_{80}Pd_{20}$	–	–	90		[94]
$Zr_{55}Al_{10}Ni_5Cu_{30}$				Break or split	[93]
$Ti_{50}Cu_{20}Ni_{23}Sn_7$				Break or split	[93]
$Fe_{65.5}Cr_4Mo_4Ga_4P_{12}C_5B_{5.5}$				Break	[95]

necking and cavitation. From initial stable homogeneous deformation to unstable flow, MGs experience instability. How do different kinds of deformation instabilities occur, and how do they evolve and result in the final fracture? Over the last decades, researchers have paid great attention to these fundamental questions and provided deep insights into the origin and propagation of shear banding, the formation and growth of cavitation, shear band multiplication and necking. Moreover, the analysis of the crack tip field provides a new perspective on the inherent connection between macrodeformation and micromechanisms.

3.1 Shear banding

One of the major micromechanisms in the deformation of MGs is inhomogeneous deformation by concentrating severe plastic strain into nanoscale shear bands [1-3,15,28,37,43,100,108-112]. As precursors to crack formation, the localized plastic regions render very limited ductility before catastrophic failure under unconstrained loadings, such as tensile testing [87]. Under constrained loading, such as compression, indentation and bending, the shear banding process does not always behave in a runaway manner but in a stable serrated flow mode through shear band multiplication [29,62,86,113,114]. The nature of shear banding, referring to its formation, propagation and multiplication, is critical to reveal the mechanisms underlying the failure of MGs. To date, there have been significant advances in understanding the behavior of shear bands in MGs, and numerous works have focused on the origin and propagation of individual shear bands [12].

Although how shear banding of MGs originates from the

atomic structure still lacks a precise physical picture, it is well accepted that the formation and self-organization of flow events, which are essentially local arrangements of atoms around free volume sites, termed STZs or flow defects [2,3,115-119], lead to shear localization [11,117,120,121]. Both theoretical and experimental studies have demonstrated the localized and cooperative nature of shear transformation [3,115,122]. The specific characteristics of STZs have been widely investigated [122-125], i.e., their shape and size, the activation energy for the transformation, their correlations with local structure and the macrodeformation. Pan et al. [122] reported experimental characterization of STZs for MGs. They investigated the activation kinetics of shear transformations by nanoindentation at different rates, and the activation volume was derived from the strain-rate sensitivity. The STZ volumes of the selected MGs were then estimated to vary from 2.5 to 6.6 nm^3 based on the cooperative shearing model of Johnson and Samwer [115]. Generally, STZs in MGs require activation energy of several tenths of eV and display a diameter of ~1 nm, which contains a few tens to a few hundred atoms. It has been suggested that a large STZ volume facilitates plasticity [122,126]. Due to the extreme tempo-spatial scale of shear banding, the atomistic mechanism of plastic localization is difficult to properly resolve by experimental means, and computational simulations provide a powerful tool to unveil the shear banding mechanism at the atomic level. Simulations show that STZs prefer to activate in regions involving weakly bonded atoms. As their induced elastic fields have long-range interactions with each other, STZs prefer to occur as directional quasi-linear avalanches rather than as independent, random events [123,124]. Şopu et al. [127] identified how an STZ generates a structural perturbation in the surrounding material and then triggers the activation of the neighboring STZ. The catalytic self-assembly of STZs is illustrated in Fig. 1, which reveals a two-unit mechanism for STZ percolation. The autocatalytic generation of successive strong strain and rotation fields induces STZs to percolate each other and then leads to the formation of a shear band. From the perspective of the strain gradient, Tian et al. [128] proposed that structural heterogeneity, or more specifically, the strain gradient, drives the coalescence of the existing activated regions, eventually initiating shear bands. As displayed in Fig. 2, the local fivefold symmetry (L5FS) and the local von Mises strain (η^{Mises}) evolve with the macroscopic shear strain γ. In the beginning, STZs are mostly activated in low L5FS regions (Fig. 2a), and as deformation proceeds, STZ activation regions are broadened and coalesce along some specific directions (Fig. 2b). The strain gradient fields (Fig. 2c) and the structural features (Fig. 2b) show good consistency. Large strain gradient zones then percolate (Fig. 2d) and play a critical role in driving shear banding.

For decades, the onset condition of shear banding in MGs and its underlying mechanism have aroused considerable debate. The concept of "free volume" was introduced to describe the plastic flow of MGs, and a steady-state inhomogeneous flow model was proposed by Spaepen [1]. Free volume dynamics, i.e., Stress-driven creation and diffusion annihilation of free volume, are found to play a dominant role in shear instability [2,3,110]. A general theoretical framework was established by Huang et al. [108] to characterize the inhomogeneous deformation in MGs, where the onset condition for shear instability solely relies on free volume. Another popular viewpoint is that shear band formation in MGs is attributed to thermal softening, similar to adiabatic shear bands in crystalline alloys [79,129]. However, because of rapid thermal conduction, adiabatic heating was reported to be impossible in MGs [130,131]. Using high-speed infrared cameras, it was measured that the temperature within the shear band only rises by approximately 0.55 K within 1 ms [47]. Compared with the sole effect of free volume or heat, a thermomechanical coupled effect on shear band formation was proposed [28,132]. Several coupled thermomechanical finite-deformation constitutive frameworks were developed to model the homogeneous deformation or localization in MGs [133,134]. Dai and coworkers [28,37,132] established a new theoretical framework to describe the thermomechanical deformation of MGs. They carried out a rigorous linear perturbation analysis on three types of instabilities, namely, free-volume softening, thermal softening and coupling softening, and derived the corresponding onset criteria. It was pointed out that shear-

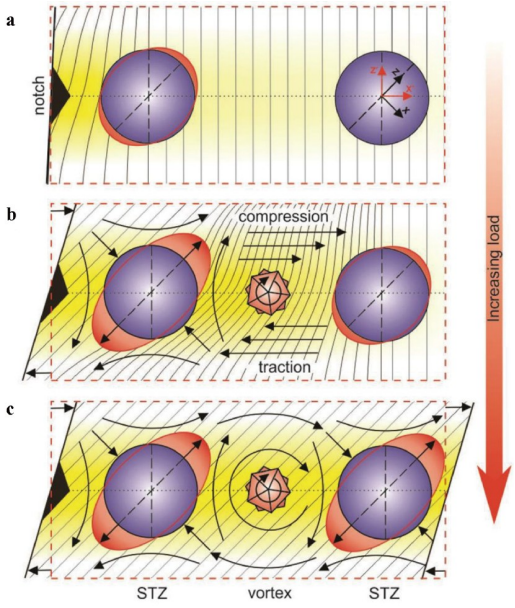

Figure 1 Illustration of the two-unit mechanism for STZ percolation: **a** at small loads, the STZ near the notch experiences a small distortion, which has a negligible effect on the neighboring matrix, **b** the STZ is activated at a higher load, and collective vortex-like motion is caused, and **c** the following STZ is activated once the stress exceeds the threshold value [127].

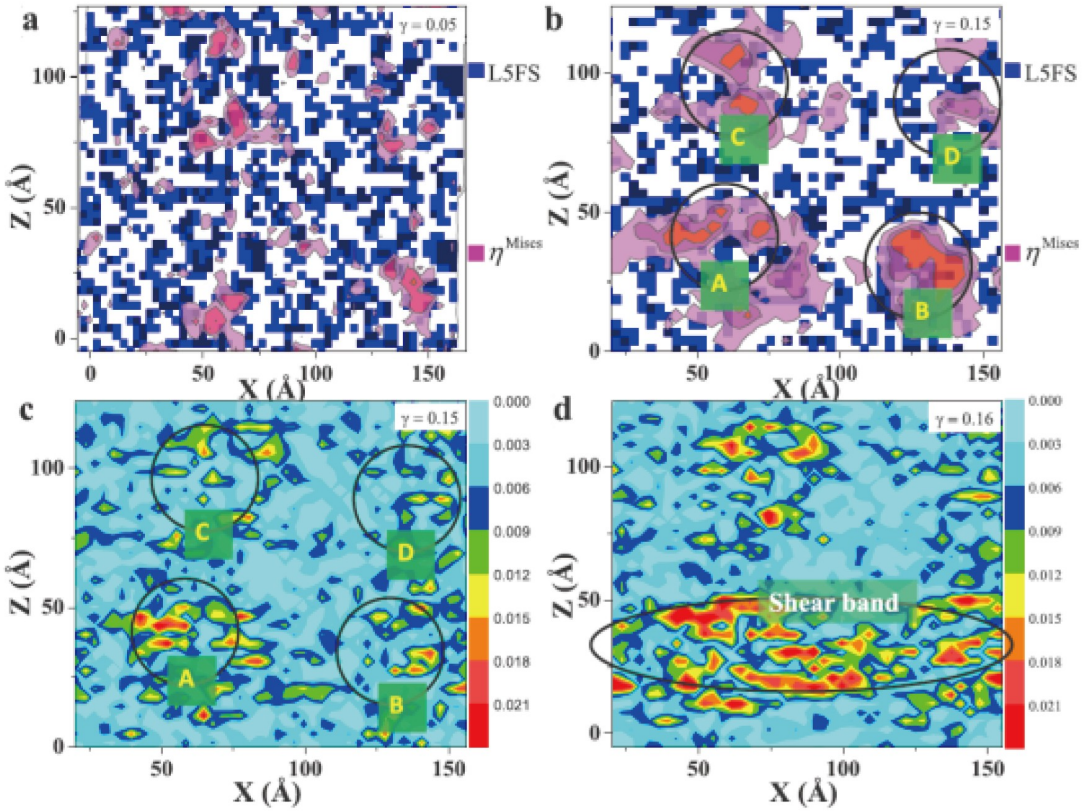

Figure 2 Evolution of local von Mises strain and L5FS with macroscopic shear strain. Deformation patterns at **a** $\gamma = 0.05$ (before yielding) and at **b** $\gamma = 0.15$ (right before the emergence of the shear band), respectively. Strain gradient fields in the z direction immediately **c** before and **d** after shear band formation, respectively [128].

band instability is attributed to coupling softening, where stress-driven free volume softening plays the dominant role while thermal softening promotes the process [37]. This mechanism was verified experimentally by Brennhaugen et al. [135]. They introduced a new experimental approach to detect the localized boiling of liquid nitrogen by the heat generated in shear banding and found that heating follows the operation of the shear band.

The direction of shear band formation as an important feature of shear banding relies on material types and loading states. As mentioned before, the shear band angles of MGs normally deviate from the direction of the maximum shear stress because the macroscopic yield behavior of MGs is pressure-sensitive and does not obey the classical pressure insensitive forms [23,64,65,73,116,136,137]. From a continuum point, shear banding is actually a physically material unstable event, which can be treated like the appearance of instability in the macroscopic constitutive description of inelastic deformation. For pressure-sensitive dilatant materials, Rudnicki and Rice [24] derived both the general onset condition and orientation of the shear band in the stress space by tying the bifurcation theory. Based on this, Gao et al. [138] predicted the shear band angle for MGs, where the pressure coefficient and the dilatancy factor play critical roles. Ruan et al. [139] established a constitutive model addressing the physical origin of shear banding, where the atomic structural change was embodied by the plastic strain and the associated dilatation for MGs. They derived the conditions for the onset of shear banding instability, which enables the explicit calculation of the shear band inclination angle. New constitutive accounting for pressure sensitivity, dilatancy and structural evolution was introduced by Chen and Dai [140]. Combining the bifurcation theory, they derived the critical condition and direction for shear band formation in MGs under a general stress state, which connects the microscopic origin and the loss-of-ellipticity instability in the constitutive law in continuum mechanics.

Once initiated, the shear band will propagate and result in subsequent fracture; therefore, the propagation speed and mode are basic issues to be determined. Early experiments on shear band speed were carried out by using high-speed cinematography or linear variable differential transformers [141]. However, due to the limitations of the temporal and spatial resolution, only a few and limited datum points were recorded and were not sufficient to determine the shear band speed. To improve it, Song and Nieh [41] introduced strain gauges capable of capturing small strains (~10^{-5}) with a high data acquisition rate (~2000 Hz) and directly measured the

strain change as a function of time during compression tests of Zr-based MGs. Microsize serrations were found in the obtained displacement-time curves, in which a three-step (acceleration, steady-state, and deceleration) process was uncovered in shear band propagation. The shear band speed varies in different stages, and the maximum is calculated to be 800 μm/s. Wright et al. [142] measured the temporal and spatial evolution of strain during the serrated flow of Pd-based MGs under quasi-static compression through a similar but advanced experimental approach. Strain gauges were affixed to all four sides of the specimen, and a piezoelectric load cell was located near the specimen. The strain and load could then be acquired at rates of up to 400 kHz. The shear band velocity was estimated to be approximately 0.002 m/s based on the assumption that the entire shear plane displaces simultaneously. If the displacement occurred as a localized propagating front, the velocity of the front was given to be approximately 2.8 m/s. The shear band speed of 1-10 m/s was also calculated by combining the acoustic emission method [143]. Regarding the actual mode of shear band propagation, there are two viewpoints following that of Wright et al. [142]. One considers that shear occurs simultaneously across the entire shear plane, termed the shear displacement jump mechanism [38-41]. The other favor is that the shear front progressively propagates across the shear plane from one end of the sample to the adjacent free surface, analogous to crack propagation [29,42-45]. To verify these two viewpoints, different experimental evidence has been claimed. The support of the latter scenario stems from *ex situ* observations of diffuse shear bands that do not extend fully across but terminate within the sample [111,143]. Song and Nieh [41] found the growth rates of the shear offsets on either side of the sample to be equal, supporting the former mechanism. The serrated flow in the compression of MGs was attributed to an intermittent, stick-slip mechanism with repeated cycles of initiation, propagation, and arrest [38,40,41,117,144].

Instead of individual dominant shear bands, multiple shear bands are found in the deformation of MGs under constrained loads along with considerable plastic deformation. Due to its remarkable improvement of plasticity, shear band multiplication has aroused intense scientific and technological interest from scientists [16,30,62,113,117,139,145-147]. In MGs, there are several ways to realize shear band multiplication, such as introducing structural heterogeneity [57,148-154], adopting constrained loading modes [16,30,62,111,113,145,155,156], or controlling the sample size and machine stiffness [42,43,157]. In the multiplication process, two basic processes are involved, i.e., shear band nucleation and growth. The former triggers the production of new shear bands, while the latter will speed the failure of MGs. Analogous to those observed in crystalline metals, multiple sets of shear bands in MGs are organized in characteristic patterns, where the shear band spacing and offset vary with global strain, strain rate, normal stress, and sample dimension [29,30,86,133,147]. A strong size effect on multiple shear bandings has been revealed in MGs [16,29,145].

To predict shear band spacing, several prevailing theories, which are original for multiple thermoplastic shear bands of crystalline metals, have been developed by Grady and Kipp [158], Grady [159,160], and Wright and Ockendon [161]. Based on these pioneering works, the early models for shear band spacing and offset in MGs are usually based on momentum diffusion or energy balance. Conner et al. [145] demonstrated that shear band spacing and offset scale with the thickness of the MG plate under bending due to a strain relaxation near the shear band. Considering a balance between the energy dissipated along with shear bands and the macroscopic dissipation, Ravichandran and Molinari [16] proposed an analytical model to predict the scaling laws of shear band spacing and offset in MGs over a wide range of size scales when subjected to plane-strain bending. A thermomechanical model based on momentum diffusion was established for the evolution of shear band spacing in MGs under dynamic loading, and it was revealed that normal stress plays a crucial role in shear band formation [147]. Wei et al. [162] extended the analysis by Conner et al. [145] of bands in bent plates. By introducing the micromechanics of individual shear bands, they found that both shear band spacing and offset decrease as Poisson's ratio increases toward a more uniform deformation.

Significant size effects and tension-compression asymmetry are presented in the self-organization of collective shear bands in MGs under *in situ* four-point bending tests [29]. From three basic processes, namely, momentum diffusion, energy conservation and structural evolution, Chen et al. [29] developed an analytical model for the evolutionary dynamics of multiple shear banding for MGs. They derived the analytical solutions of shear band spacing, shear offset, and failure strain for the bending case, which is in good consistency with the experimental observations. The inhomogeneous size effect of plasticity is revealed by a transition from weak ($(h^*)^{-2/3}$) to strong ($(h^*)^{-2}$) size dependence of failure strain with decreasing sample thickness h^* (Fig. 3). In the figure, Δu is a critical value of the shear offset. The shear band is assumed to transform into a mixed mode crack when the shear offset in the mature shear band exceeds Δu [16,145]. Both prediction lines for different values of Δu show the same change trend, but the blue line for larger Δu exhibits a better plastic deformation capability. To uncover the underlying mechanism of the cooperative behavior of multiple shear bands, an energy competition map was proposed based on the energy dissipation by shear band nucleation and propagation. As elucidated in Fig. 4, the energy dissipated per unit change of shear band spacing (measured by $\Gamma_\lambda^* / \Gamma_0^*$, in the blue curve) or shear offset (characterized by

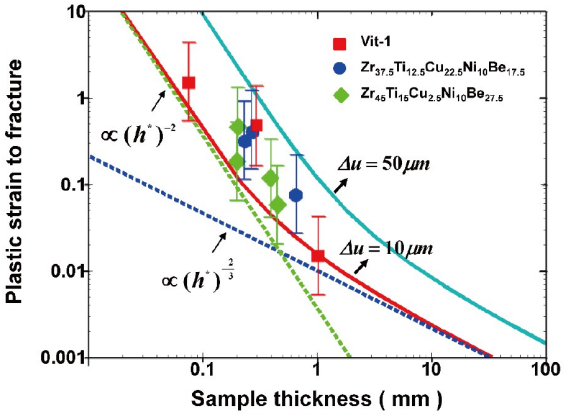

Figure 3 Plastic strain to fracture varies with sample thickness for Δu = 10 μm (red solid line) and Δu = 50 μm (blue solid line). The analytical prediction is consistent with experimental data [146] for Vit-1 and other similar compositions [29].

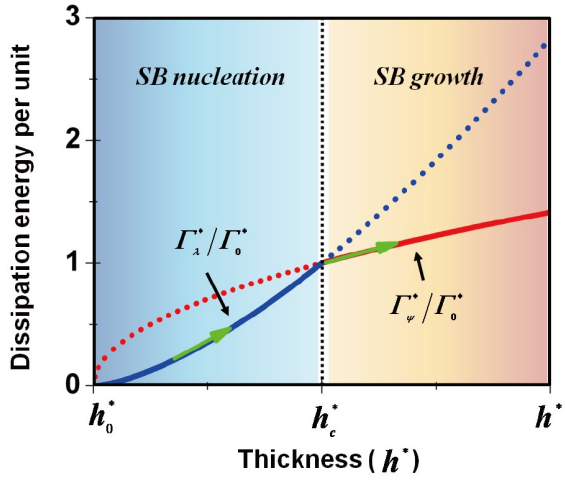

Figure 4 Energy dissipation map for shear band nucleation and growth as a function of sample thickness [29].

$\Gamma_\psi^* / \Gamma_0^*$, in the red curve) varies with the sample thickness h^*. Both energies grow monotonically with increasing h^* and equal to Γ_0^* at the critical sample thickness h_c^*. The competition between these two dissipation energies determines which process takes priority. This result indicates that shear band nucleation would be more active when $h^* < h_c^*$, while shear band propagation plays a dominant role when $h^* > h_c^*$. The transition from shear band nucleation to propagation is in accordance with the variation in the size dependence of plastic strain (Fig. 3), which provides a new insight into the size effect of plasticity in MGs.

3.2 Necking

To attain a better plasticity, multiple shear bands or even homogeneous plastic deformation is preferred in MGs. Although most MGs show negligible tensile ductility under tension, superplasticity has been obtained under special conditions through a ductile fracture mode of necking. During necking, the material experiences homogenous deformation before the final fracture. A reduction in material size will promote shear band multiplication or even cause a transition from shear localization to homogeneous deformation when the size is reduced to hundreds of nanometers [22,27,163-168]. Once the sample size is smaller than the critical value of shear band thickness, a shear band cannot be formed, and homogeneous plastic flow and necking instability occur [165]. Guo et al. [27] presented significant uniform elongation and extensive necking behavior in Zr-based MGs with dimensions on the order of 100 nm by using an *in situ* tensile test in a transmission electron microscope (TEM) (Fig. 5). Jang and Greer [167] reported a superior strength of 2.25 GPa and ductility of ~25% in 100 nm-diameter Zr-based MG nanopillars. They pointed out that a highly localized-to-homogeneous deformation mode change occurs at a 100 nm diameter and presented a phenomenological model of two competing processes for brittle-to-homogeneous deformation. This critical length scale on the order of ~100 nm was further confirmed by Zhou et al. [168] through atomistic simulation and theoretical analysis. They proposed that the critical size required for the transition from shear banding to homogeneous deformation in MGs is determined by shear band energy and surface stress. At high temperatures close to or above the glass transition, MGs usually experience homogeneous viscous flow. These size- and temperature-dependent deformation properties suggest that applications on small

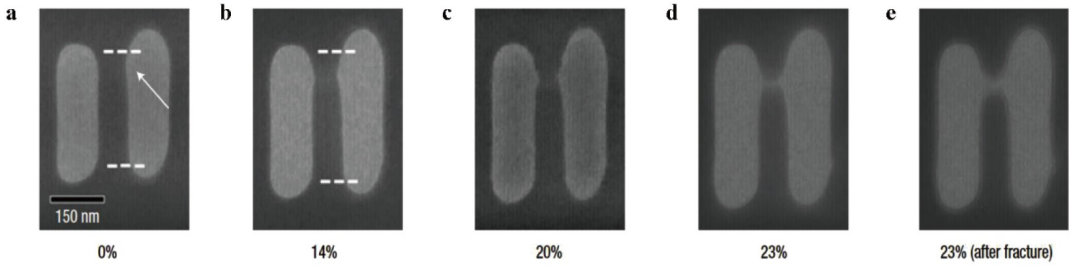

Figure 5 MGs experience necking behavior during the *in situ* TEM tensile tests. Necking starts early from the "notches" on the surfaces in the virgin sample (indicated by the white arrow in **a**) and then **b-d** develops gradually to **e** final failure [27].

length scales or high temperatures can take advantage of the enhanced plasticity of MGs [166].

In addition to the extrinsic factors (i.e., sample size, temperature), ductility can also be improved by adjusting the intrinsic factors (i.e., microstructure). Hofmann et al. [148] introduced MG-matrix composites with enhanced global ductility and necking failure. The inhomogeneous microstructure with isolated dendrites would impede the extension of shear bands and promote the formation of dense multiple shear bands, which effectively stabilizes the glass against catastrophic failure and leads to relatively homogeneous deformation before final failure.

3.3 Cavitation

Ductile to brittle transition has been widely reported in the deformation of MGs [15,50]. This is not only reflected by the macroplasticity but also strongly suggested by the observation of distinct fracture surface morphologies in MGs [15]. Coarser patterns are usually found in ductile fracture surfaces with deep ridges on the micrometer length scale, while nanoscale periodic corrugations are exhibited in brittle fracture surfaces. Through statistical characterization of fracture surfaces, Bouchaud et al. [169] reported exotic multiaffine isotropic scaling properties of the fracture surfaces in Zr-based MGs. The mismatch between the two facing fracture surfaces shows that fracture occurs mostly through the growth and coalescence of damaged cavities. Jiang et al. [15] conducted systematic compression, tension and high-velocity plate impact experiments on a typical Zr-based MG. An obvious change in fracture patterns with the strain rates was observed. At a high strain rate, it was interesting to find nanoscale dimples and periodic corrugations in tough MGs. After a broad overview of the fracture patterns of specimens, a criterion was proposed to predict whether the fracture of MGs is brittle or plastic, which depends on the curvature radius of the crack tip and the critical wavelength of meniscus instability. If the former is greater than the latter, microscale vein patterns and nanoscale dimples appear on crack surfaces; otherwise, local quasi-cleavage with local softening dominates and produces nanoscale periodic corrugations. The classical STZ is a fundamental unit process underlying plastic softening but is not sufficient to explain these two distinct phenomena. A collective atomic motion, namely, TTZ, was then proposed as the basis of quasi-cleavage (Fig. 6). Energy dissipation in the fracture of MGs was revealed to be determined by STZs and TTZs ahead of the crack tip. The alternative activation of TTZs and STZs in front of the crack tip causes the arrest and propagation of a mode I crack, resulting in the formation of periodic corrugations. A ductile-to-brittle transition was also found during the spallation of a binary MG [36]. The interaction between void nucleation and growth, which at the atomic scale originates from competition between TTZs and STZs, was revealed to control this transition.

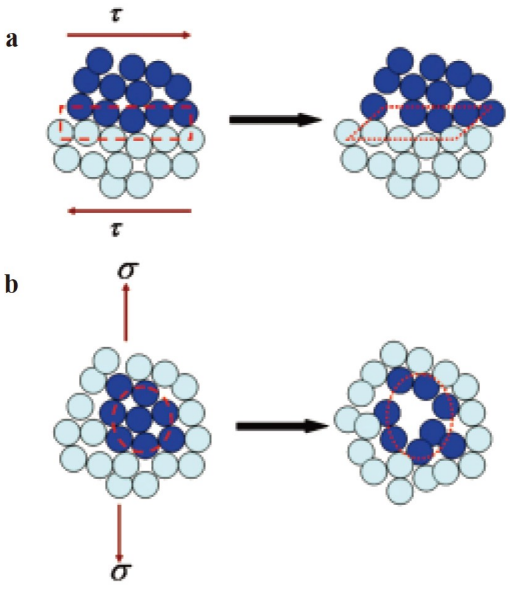

Figure 6 Schematic of two fundamental atomic motions in MGs: **a** a classical STZ and **b** an envisioned TTZ [15].

Early in 1945, Bishop et al. [170] recognized the existence of cavitation instabilities and presented cavitation limits in elastic-plastic solids under stress conditions consistent with spherical and cylindrical symmetries. Thereafter, limit states for cavitation under symmetric stress states or general axisymmetric stressing were analyzed [171-173]. As a ductile failure mechanism under highly constrained plastic flow, cavitation instabilities are usually considered a process in which elastic energy stored in the remote field drives the plastic expansion of the void [173]. However, quite a different case is found is MGs. The cavitation mechanism of the fracture behavior in brittle MGs was unveiled by Murali et al. [33] through atomistic simulations. In contrast to extensive shear banding leading to ductile failure in the CuZr MGs, an intrinsic cavitation mechanism near crack tips governs brittle fracture in FeP glass (Fig. 7). The main reason for the observed cavitation behavior in the brittle MGs is attributed to a high degree of atomic-scale spatial fluctuations in the local properties. Further simulations by Murali et al. [174] showed that spontaneous cavitation in MGs tends to occur preferentially inside an inclined localized softening zone emanating from a crack tip or under unequal biaxial tension, and the nucleation and coalescence of the cavity then cause the crack to extend and lead to brittle fracture. The spatially fluctuating curvature-dependent surface energy, termed the Tolman length effect, was also found to be an important factor influencing cavitation in MGs [175]. Huang et al. [176] unveiled that sites with loose packing atomic clusters in MGs would facilitate the nucleation of microvoids. Recently, the cavitation mechanism underlying the fracture

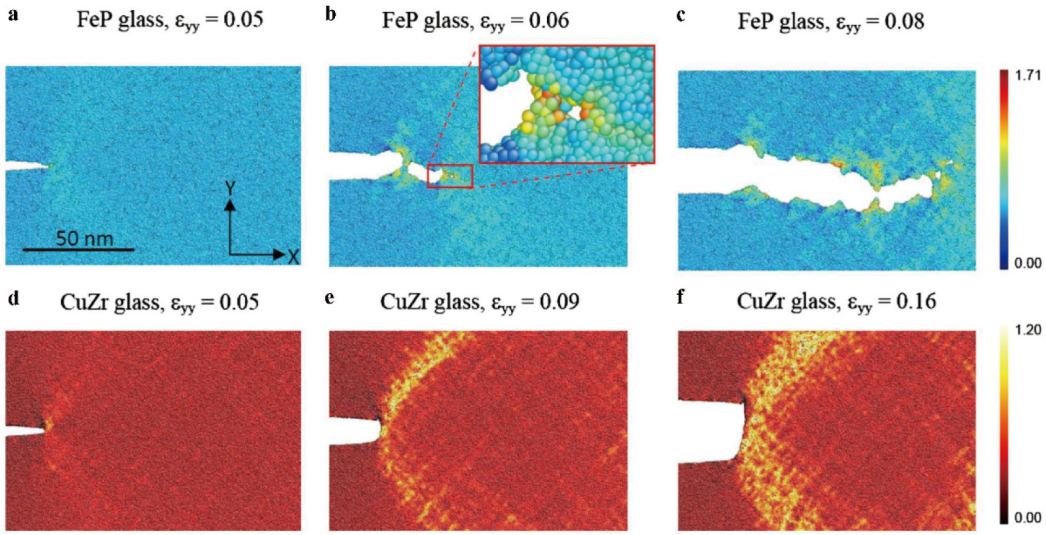

Figure 7 Numerical results of crack propagation at various applied strains in **a-c** Fep glass and **d-f** CuZr glass. The color indicates the local von Mises strain [33].

behavior of glasses was verified experimentally by Shen et al. [177]. They experimentally presented the cavitation-dominated cracking process in MGs through a precise characterization of the nucleation, growth, and coalescence of growing cavities (Fig. 8). Further studies were carried out in nonmetallic PC and SiO_2 glasses, where cavitation-induced nanopatterns are also prevalent, suggesting the presence of nanoscale ductility in the macroscopic brittle fracture of glasses. This work provides a direct and clear picture of how fractures proceed in glasses and paves the way for a deep understanding of the failure of disordered materials.

To explain these cavitation behaviors in MGs, several models of cavitation instability, void nucleation and growth have been developed [21,32,34,178-180]. The first continuum model of cavitation for MGs was established by Huang et al. [178]. They introduced a single-stage light gas gun and designed a special plate-impact experiment. Through impact tests on a Zr-based MG, microvoids were found to nucleate in the material during spallation. Based on free-volume theory, they proposed a microvoid nucleation model of MGs and revealed that nucleation of microvoids at the early stage of spallation in MGs is attributed to diffusion and coalescence of free volume, in which high mean tensile stress plays a dominant role. Thereafter, Huang et al. [179] further presented a theoretical description of cavitation instabilities and void growth dynamics undergoing remote hydrostatic tension. An explicit expression of the critical pressure for cavitation instability was derived from theoretical analysis of the material elastic-viscoplastic response. As shown in Fig. 9, cavitation instability prefers to occur in solids with a relatively high-pressure sensitivity coefficient. To characterize the dominant factors in dynamic void growth, they proposed a dimensionless number, which consists of three different time scales (namely, the inertial time scale t_{inertial}, the loading time scale t_a and the relaxation time scale t_r). Via finite difference method simulations, see Fig. 10, it was found that at the rise stage of the loading history, the growth process is governed by the competition between the inertial effects and the loading rate effects. The dominant factor transitions from inertial effects to viscous effects when $I_1 = t_{\text{inertial}} / t_a < 10^{-2}$. When the viscous effects start to work, the loading rate effects are gradually weakened, leading to a higher void growth rate and the disappearance of vibrating growth. The growth process is manipulated by the competition between the inertial effect and the viscous effects at the steady stage. A transition is at $I_1 = t_{\text{inertial}} / t_r = 1$, above which the inertial effects play the major role and the growth of voids is restricted. Otherwise, void growth is controlled by the viscous effect. Moreover, the influences of the surface energy and thermal effects on void growth were discussed by introducing dimensionless numbers I_γ and I_{th} [180]. I_γ denotes the ratio of the energy required to form a new void surface and the energy dissipated by plastic deformation, and I_{th} represents the competition between momentum diffusion and thermal diffusion. The surface energy was found to significantly restrict void growth at the early stage when I_γ was large, while the thermal effects first promoted and finally impeded void growth at the late stage when $I_{\text{th}} \leq 1$. It elucidates the coupling influences of inertia, surface energy and thermal effects on void growth and the dominant factors as the process develops.

Material properties in a brittle MG normally exhibit large spatial fluctuations, which are considered a reason for the nucleation and coalescence of nanovoids [32,33,176]. Singh et al. [32] introduced weak zones and proposed a model of a

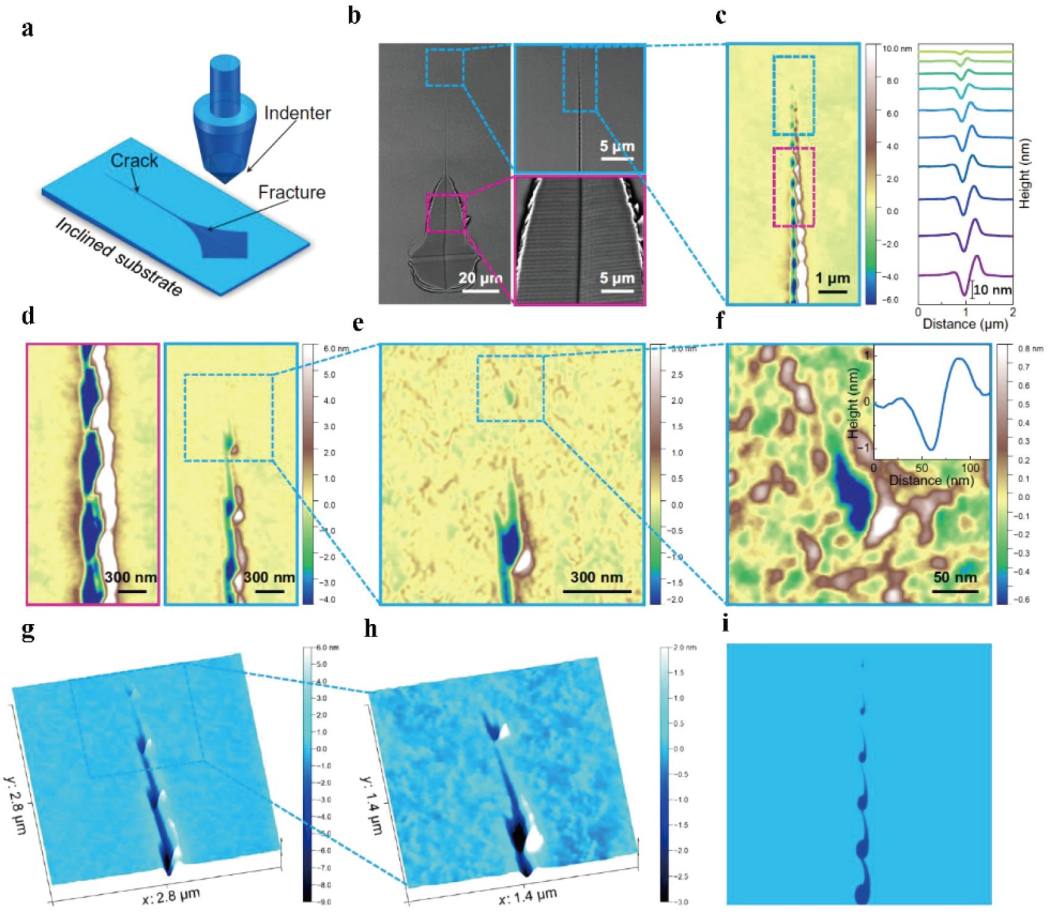

Figure 8 Experimental observation of the cavitation-dominated fracture process in the Fe-based MG. The experimental setup of inclined indentation is illustrated in **a**. **b**, **c** Scanning electron microscope images, atomic force microscope topographic image of the zoom-in straight crack (left) and height profiles of the top 10 cavities (right) after inclined indentation, respectively. **d** Zoomed-in topographic images of the pink (left) and blue (right) rectangular zones in **c**. **e**, **f** Topographic images of the crack tip and the cavity ahead of the crack tip, respectively. Inset: height profile of the cavity. **g**, **h** Three-dimensional close-up topographies of another crack tip. **i** Crack propagation [177].

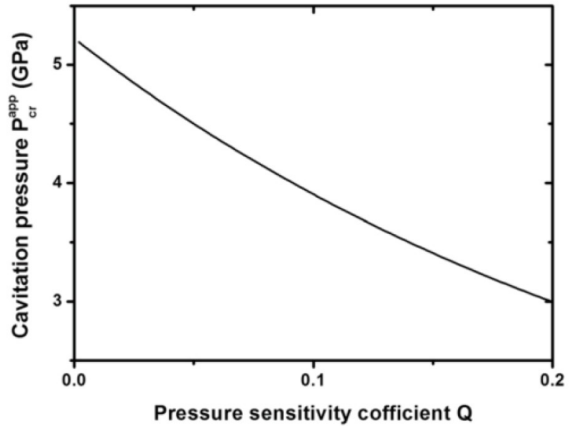

Figure 9 Cavitation pressure decreases with increasing pressure sensitivity coefficient [179].

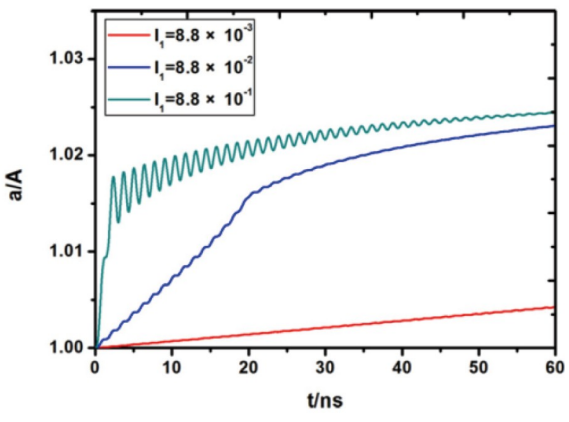

Figure 10 Void growth for different rise times with an initial void radius of 1 μm under the same loading amplitude of 2 GPa [179].

heterogeneous solid to represent a brittle MG. In their model, the weak zones are treated as periodically distributed regions that have lower yield strength than the background material. It was found that the local yield properties of the weak zones control the critical hydrostatic stress for the onset of cavitation, and this stress threshold is greatly reduced by the presence of these zones. Moreover, the applied stress state was revealed to be another important factor influencing the

cavitation behavior of such a heterogeneous plastic solid with distributed weak zones [34], and it showed that the cavitation stress of the heterogeneous aggregate is controlled by the critical value of a nondimensional stress state parameter. The cavitation mode would experience a transition from snap cavitation or smooth bifurcation at a high stress ratio to unstable bifurcation at a sufficiently low stress ratio.

3.4 Crack-tip fields

Crack-tip fields are crucial in studying the fracture of solids. There are a number of significant works on the theoretical solutions of crack tip fields for ideally plastic and power-law hardening materials. One of the most famous works is from Rice [181], who raised the path independent *J*-integral as an average measure of the crack tip field for elastic and elastic-plastic materials. Combining the *J*-integral and the slip line field analysis, an approximate solution of the plastic zone was derived for perfectly plastic material [181]. The well-known Hutchinson-Rice-Rosengren (HRR) singular fields were then established for a power hardening material [182,183]. Based on the HRR-type fields, the crack-tip stress and strain fields with volume preservation of deformation were presented by Pan and Shih [184,185] for power-law hardening orthotropic materials under plane-strain and plane-stress conditions. Considering volumetric deformation, Hutchinson [186] proposed crack tip fields of the HRR type for polycrystalline materials undergoing creep-constrained grain boundary cavitation. Theoretical and numerical methods have been developed to evaluate the stress intensity factors (SIFs) ahead of the crack tip [187-189]. Recently, for arbitrarily sized kinked cracks, Liu and Wei [190] established a theoretical framework to calculate the stress fields and hence the SIFs. For amorphous solids, pressure sensitivity and dilatancy are two important traits in deformation [23,64,140]. Li and Pan [25,26] introduced a pressure-sensitive yield criterion and the normality flow rule to describe the deformation of pressure-sensitive dilatant materials, and derived solutions of the crack tip stress and strain fields for plane-stress and strain conditions, respectively. Jeong et al. [191] constructed theoretical slip lines around notches for pressure-sensitive perfectly plastic material by utilizing the Drucker-Prager yield criterion. Softening and orientation hardening were incorporated into a viscoplastic constitutive model for glassy polymers, and a finite deformation analysis of the crack tip fields was performed [192]. For pressure-sensitive plastic solids, a 3D finite element analysis of mode I crack tip fields was conducted by Subramanya et al. [193] under small-scale yielding (SSY) conditions. These works might provide a theoretical basis and useful methods for the study of crack tip fields in MGs.

Early works referring to the crack tips of MGs focused on their correlation with fracture toughness. Lowhaphandu and Lewandowski [194] carried out single-edge-notched bending experiments on MGs with various notch radii, and the fracture toughness was revealed to increase linearly with the square root of the notch-root radius. Through tensile tests on notched bars of Vit-1 MGs, Flores and Dauskardt [23] found flat fracture surfaces in the central region but a "shear lip" near the edges of the notch root. At some point in the interior of the notched region, the mean positive stress attains a critical value that leads to void nucleation. Compared with the low fracture toughness reported in mode I loading, a much higher mode II fracture toughness was measured, which indicates that normal or mean stresses play a significant role in the deformation process at the crack tip [47]. The crack field behavior of MGs under both mode I and mixed mode loading was investigated by Tandaiya et al. [20] through four-point bending. Figure 11 shows the process of shear band-mediated plastic flow followed by crack initiation at the notch root for the mode I case. From the fractographs, the critical size of the process zone of ~60 μm was identified. What is interesting is that within this critical size, cracks grow stably inside a dominant shear band, irrespective of the structural state and mode mixity.

Many quantitative understandings of the crack tip behavior for MGs were mainly from numerical simulations. Tandaiya et al. [48,49] carried out finite element simulations to study

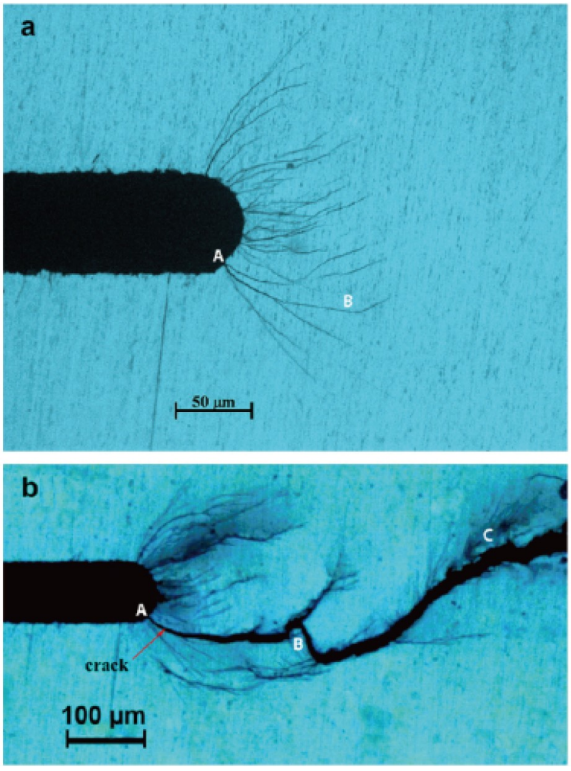

Figure 11 Optical micrographs of the shear bands ahead of **a** the notch tip in the mode I case before crack initiation and **b** the crack trajectory along the curved shear band ABC [20].

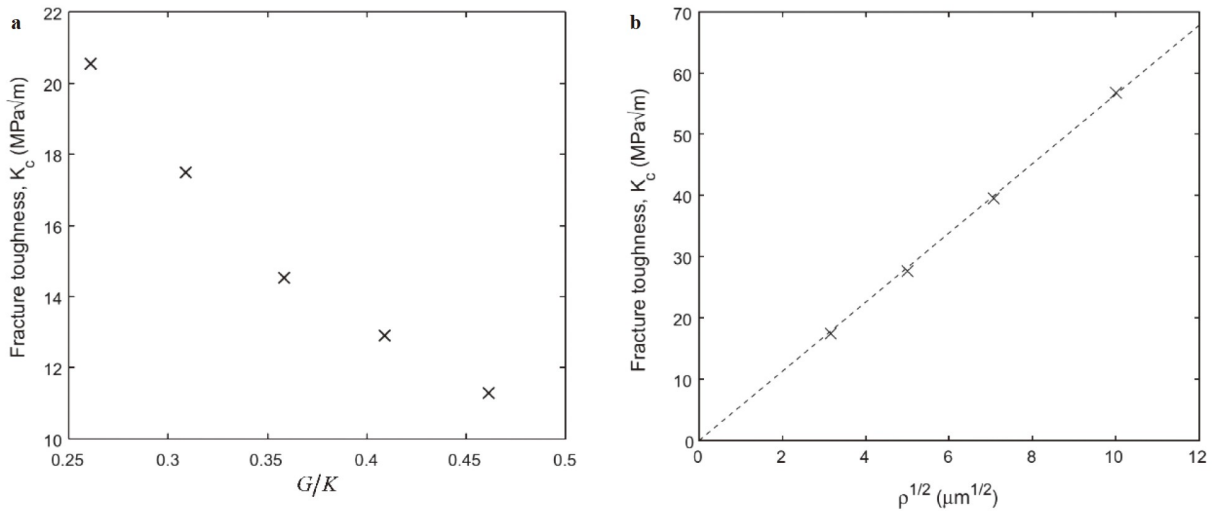

Figure 12 The variation of plane-strain fracture toughness **a** with the ratio G/K and **b** with notch-root radius [196].

mode I crack tip fields in MGs under plane-strain and SSY conditions, incorporating a continuum elastic-viscoplastic constitutive theory developed by Anand and Su [195]. According to their simulations, higher internal friction is revealed to enhance the plastic strain ahead of the notch tip but lead to a substantial decrease in the opening stress, which enlarges the plastic zone and promotes toughening of MGs. In contrast, a higher value of Poisson's ratio refers to a smaller plastic zone and plastic strain ahead of the notch tip. Henann and Anand [196] modified the Anand-Su theory to account for the softening and dilatational volumetric elastic response of MGs. Detailed finite-element simulations were conducted to investigate fracture initiation at the notch tip in MGs under mode I, plain-strain, and SSY conditions. They predicted that the fracture toughness increases linearly with the square root of the notch tip radius and decreases as the ratio of the elastic shear modulus to the bulk modulus G/K increases, consistent with those observed in experiments (Fig. 12) [196].

Mix-mode (I and II) crack-tip fields of MGs were investigated by Tandaiya et al. [19] for plane-strain and SSY conditions. The mode II component of loading was found to be an important influencing factor on crack tip behavior. As it increases, the maximum plastic zone extent is greatly enhanced, the stresses are lowered and the plastic strain levels are significantly improved near the notch. The influence of internal friction on the plastic zones, notch deformation, stress and plastic strain fields was examined as a function of the mode mixity parameter. Rycroft and Bouchbinder [197] used a simple version of the STZ model coupled to an advanced Eulerian level set formulation to analyze the crack tip behavior of a blunted straight notch under plane-strain conditions in MGs. The existence of an elastoplastic crack tip instability for sufficient relaxed glasses was revealed to cause a marked drop in fracture toughness.

Theoretical work on the crack tip plastic zone of MGs was conducted by Chen and Dai [46]. Different from the traditional theoretical description of the plastic zone, pressure sensitivity μ, shear dilatancy β and structural evolution were introduced to analyze the plastic zone in MGs. An analytical solution of the plastic zone for mode I cracks under plane-strain conditions was first derived by combining J-integral and slip line field analysis. The pressure sensitivity and shear dilatancy show obvious effects on the stress and strain distributions ahead of the crack tip (Figs. 13-15). The enhancement of pressure sensitivity and shear dilatancy would lead to a decrease in the stress components and thereby the effective and mean stresses. The shear plastic strain almost concentrated in the fan region is larger than the radial and tangential strains. Instead of a single characteristic size of the plastic zone (i.e., diameter), two characteristic length scales, namely, the maximum radius $R_{\max}$ and the radius along the crack line direction R_x, were raised, relating to shear flow instability and cavitation, respectively. The critical values of the mode I SIF and the plastic zone size at crack initiation were obtained. As shown in Fig. 16, when the value of the dilatancy factor decreases, both the fracture toughness and critical size of the plastic zone increase. When the value of Poisson's ratio increases, the fracture toughness increases, but $R_{\max c}$ has a minor change and R_{xc} decreases. Furthermore, Chen and Dai [46] proposed a dimensionless shape factor Λ_c (defined as the ratio of R_{xc} to $R_{\max c}$) of the plastic zone and presented a ductile-to-brittle transition map for MGs (Fig. 17). From the map, with the increase of β or the reduction of ν, Λ_c grows, corresponding to a variation of critical plastic zone from "slender" to "chubby". It was pointed out that different plastic zone shapes prefer different microfailure modes, and the "slender"-to-"chubby" variation of the critical plastic zone leads to the ductile-to-brittle transition in MGs.

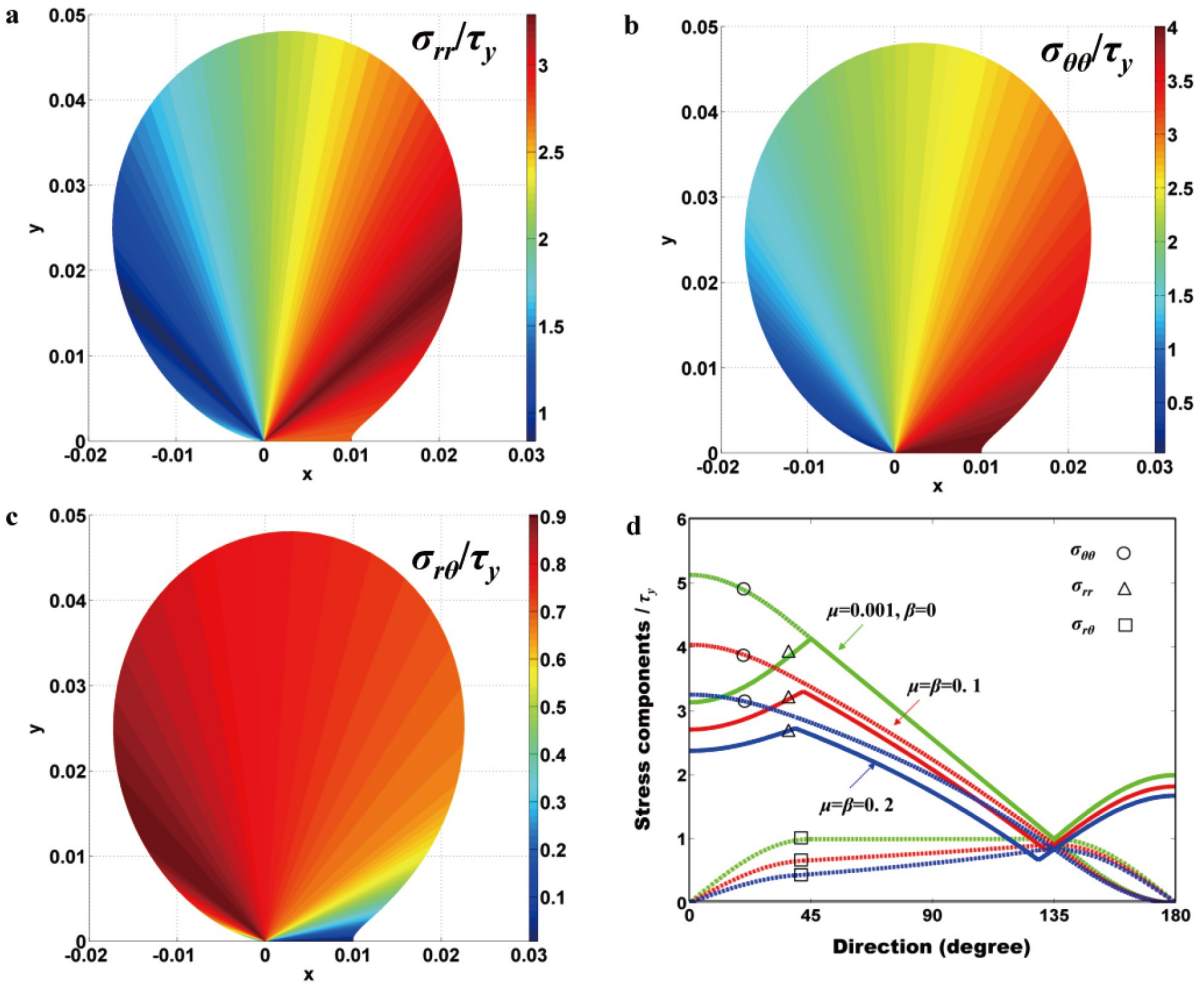

Figure 13 **a** Radial, **b** tangential, and **c** shear stress distributions in the plastic zone. **d** The angular distributions of stress components for different values of μ and β [46].

It is worth noting that the brittle versus ductile fracture mechanism in terms of cavitation and shear banding is not unique for MGs but was also reported in other amorphous materials. Ding et al. [198] performed atomic simulations on the fracture behavior of amorphous lithiated silicon and reported a brittle-to-ductile fracture mechanism transition in this material. They found that the ratio between critical stresses for cavitation and plastic yield grows with increasing lithium content, leading to a transition from intrinsic nanoscale cavitation to extensive shear banding ahead of the crack tip.

4. Inherent parameters governing ductile-to-brittle transition

Early in 1954, Pugh proposed the quotient of bulk modulus to shear modulus K/G as an indication of the extent of the plastic range for a pure metal based on a dislocation mechanism. He pointed out that a high value of K/G is associated with malleability or good ductility. Rice and Thomson [199] derived a dimensionless parameter $G\mathbf{b}/\gamma_s$ (**b** is the Burgers vector and γ_s is the surface energy) representing whether a crack is atomically sharp or blunt, and a larger value of $G\mathbf{b}/\gamma_s$ corresponds to a more brittle mode. Kelly et al. [200] predicted ductile or brittle failure in crystalline solids by the theoretical cleavage-to-shear strength ratio. They revealed that when the ratio of the maximum tensile stress to shear stress is larger than the theoretical cleavage-to-shear strength ratio, the material will fail in a pure brittle mode; otherwise, it will fracture with plastic flow. The above parameters all represent the competition between shear and cleavage through the elastic modulus or strength. From the viewpoint of the Griffith criterion, Gao et al. [201] established a critical length scale of the fracture process zone, below which the fracture strength of a cracked crystal is identical to that of a perfect crystal.

As mentioned above, a single governing parameter is normally used to characterize ductile or brittle failure in crystalline solids. For MGs, are these parameters still ef-

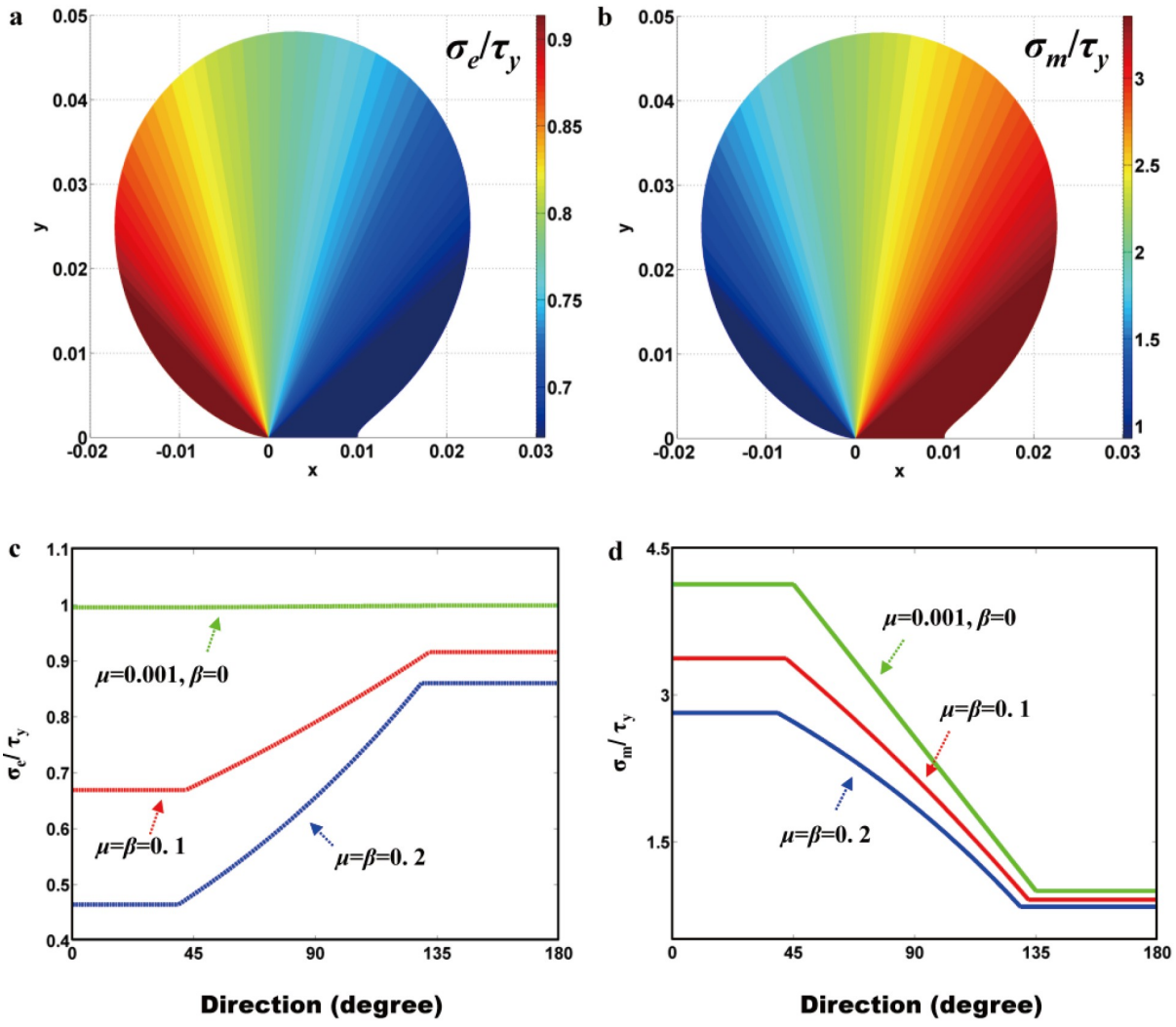

Figure 14 **a** Effective and **b** mean stress distributions in the plastic zone. The angular distributions of **c** the effective stress and **d** the mean stress for different values of μ and β [46].

fective in describing ductility? Schroers and Johnson [51] reported a pronounced global plasticity measured in monolithic Pt-based MG under both bending and unconfined compression loading conditions and suggested that the good ductility of Pt-rich MG is correlated with its large Poisson's ratio v. The high Poisson's ratio is thought to cause the tip of a shear band to extend rather than initiate a crack. Lewandowski et al. [50] collected extensive experimental data on the elastic moduli and toughness of MGs (Fig. 18) and found a similar correlation between plasticity and G/K for MGs. The critical G/K is in the range of 0.41-0.43 (or, equivalently, the critical v = 0.31-0.32*)*, where a large drop occurs in fracture energy with increasing G/K, and fracture energy approaches the toughness of oxide glasses. This intrinsic correlation between mechanical properties and elastic moduli provides an important clue to improve the plasticity of MGs by alloying with elements with low G/K or high v as constituents.

To achieve a unified description of tensile fracture in MGs, Zhang and Eckert [52] proposed a ratio of the critical normal fracture stress to the shear fracture stress, analogous to that of Kelly et al. [200]. The tensile fracture mode or ductility was revealed to vary with this ratio, and a transition was found when it reached $\sqrt{2}$ / 2.

The available theories with a single controlling factor provide significant insights into the plastic behavior in MGs. However, since a significant tension-compression asymmetry is presented in MGs [87], two or more parameters may be required to fully characterize both tensile and compressive plasticity.

In addition to Poisson's ratio, Poon et al. [202] argued that another influencing factor on the intrinsic plasticity of MGs was the local shear modulus fluctuation. They pointed out that structural relaxation could lead to dual adverse effects on ductility by increasing the local shear modulus and reducing fluctuation.

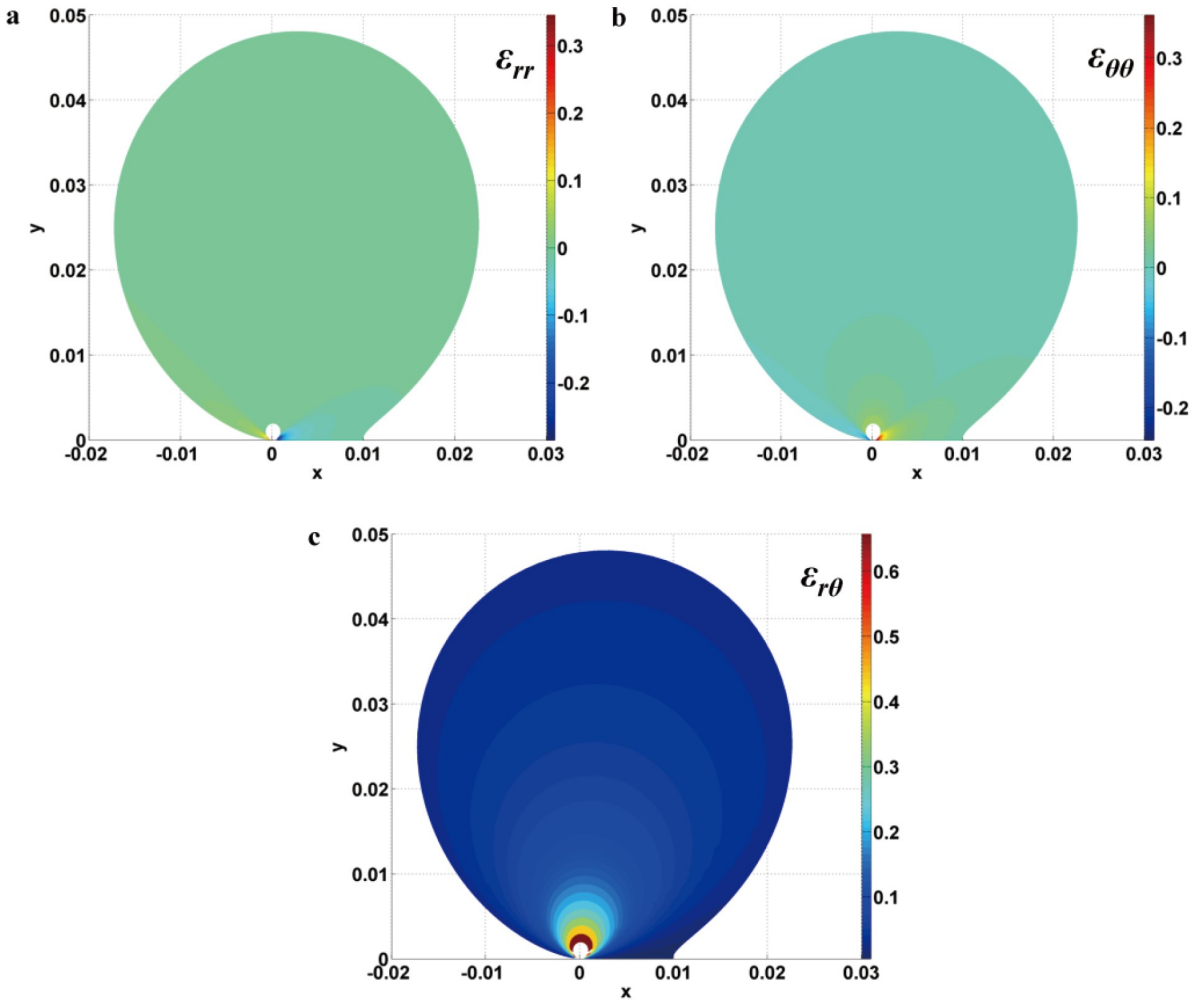

Figure 15 **a** Radial, **b** tangential, and **c** shear strain distributions in the plastic zone [46].

Taking the short-range order into account, Chen et al. [14] proposed two inherent parameters that cooperatively control whether MGs yield in a ductile manner or fracture in brittleness. One is the shear-to-normal strength ratio α characterizing the shear resistance between atomic layers. The value of α for MGs is normally larger than that of polycrystalline metals since the shear between two atomic layers in MGs always needs to push surrounding atoms apart because of the lack of long-range order and distinct slip systems. The other is the strength-differential factor β_{SD}, which measures shear-caused dilatation. The motion of an atomic cluster is illustrated in Fig. 19 [14]. Under an external load, the atomic cluster would experience shear or quasi-cleavage processes. Which one being first activated depends on the difficulty of shear (measured by α) and shear-caused dilatation (characterized by β_{SD}). Shear transformation would be easier to take place as the normal tensile strength is far larger than the shear strength. Otherwise, dilatation-induced tension would cause bond rupture in a quasi-cleavage manner due to weak atomic bonding (Fig. 19).

5. Failure criteria

The classical Tresca or von Mises criteria, both of which only predict shear failure, are not satisfactory for predicting the diverse failure modes of MGs [58]. The Mohr-Column (M-C) criterion, which takes the normal stress effect into account, has been widely used in the study of the yielding or fracture behavior of MGs [64,73,87,203-205]. However, this criterion predicts that the failure plane has a symmetric deviation from 45°; in reality, an asymmetric deviation is usually observed in MGs [87,137]. For the different failure modes of MGs, how can they be described in a satisfactory and unified fashion? To explain the tensile behavior of MGs, Zhang and Eckert [52] proposed a unified tensile fracture criterion for MGs, as expressed by

$$\sigma^2/\sigma_0^2+\tau^2/\tau_0^2 \geq 1, \tag{1}$$

where σ_0 and τ_0 are the critical normal fracture stress and the shear fracture stress, respectively. The tensile failure is regarded to be controlled by both the normal stress σ and the

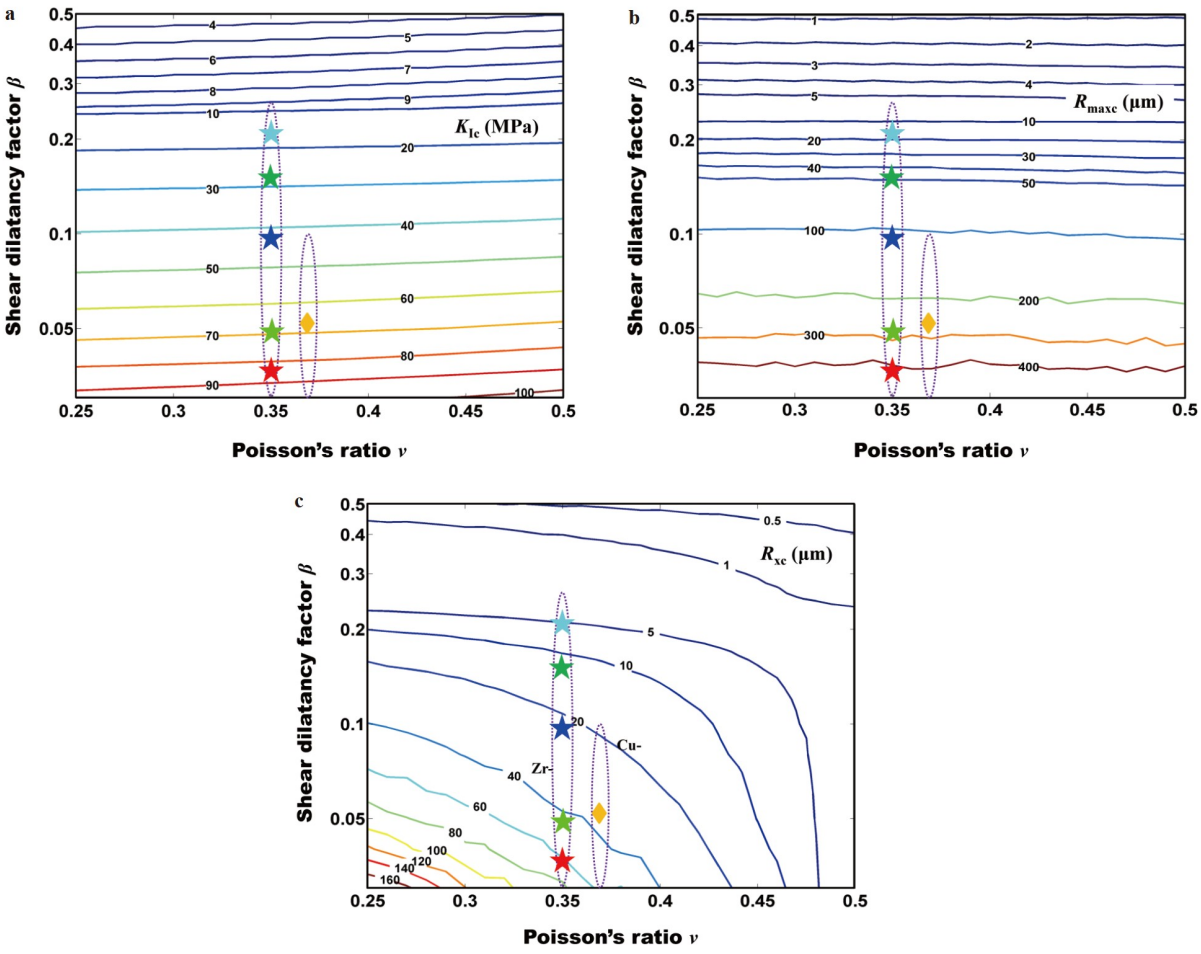

Figure 16 Isolines of mode I **a** fracture toughness, **b** R_{maxc}, and **c** R_{xc} as a function of shear dilatancy β ($\mu = \beta$) and Poisson's ratio ν [46].

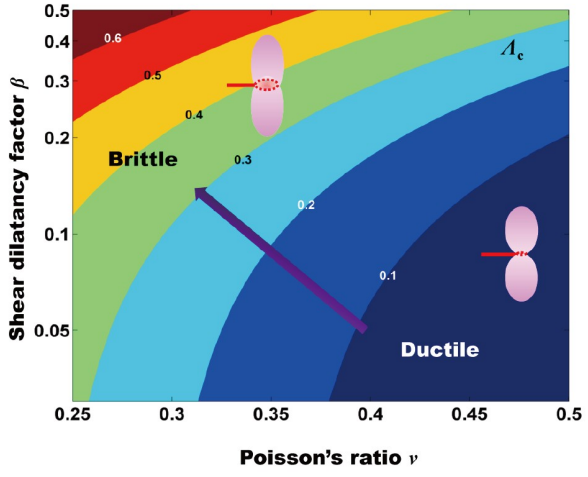

Figure 17 Isolines of shape factor Λ_c as a function of shear dilatancy β ($\mu = \beta$) and Poisson's ratio ν [46].

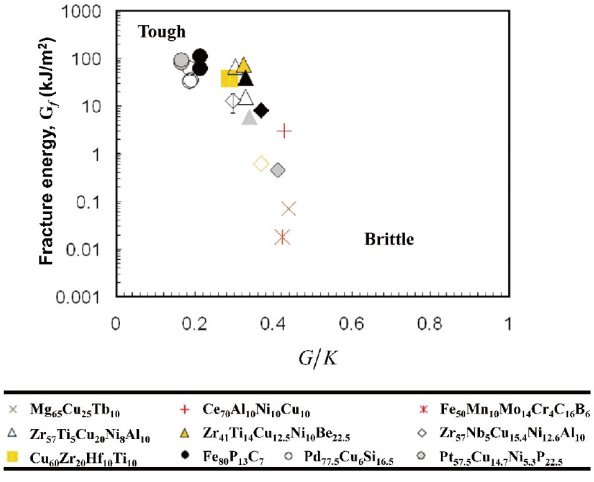

Figure 18 The correlation of fracture energy G_f with elastic modulus ratio for the as-cast MGs [50].

shear stress τ. The ratio $\bar{\alpha}=\tau_0/\sigma_0$ was raised as a critical factor that can unify various tensile fracture cases. The dependence of σ_T and θ_T on the ratio $\bar{\alpha}$ is displayed in Fig. 20. Points A and B represent the position of the Tresca criterion at $\bar{\alpha} \to 0$ and the position of the von Mises criterion at $\bar{\alpha}=\sqrt{3}/3$, respectively. The unified tensile fracture criterion predicts the Mohr-Coulomb fracture at $0 < \bar{\alpha} < \sqrt{2}/2$ (Region C) and the normal tensile fracture at $\bar{\alpha} \geq \sqrt{2}/2$ (Region D).

Qu et al. [53] introduced inclined notches with different inclination angles to a series of Zr-based MG specimens to

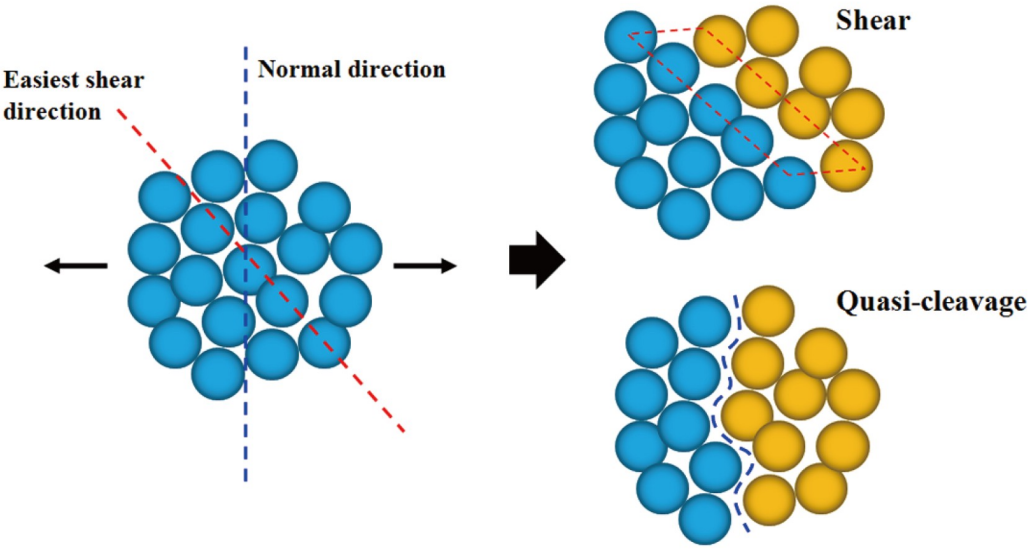

Figure 19 Schematic illustration of shear failure along the easiest shear direction and local quasi-cleavage fracture along the normal direction at the atomic scale [14].

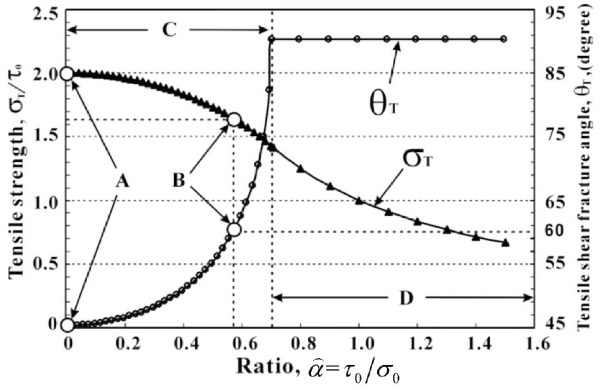

Figure 20 Tensile fracture strength σ_T and tensile shear fracture angle θ_T vary with the ratio $\hat{\alpha}$ [52].

achieve control of the normal stress acting on the tensile fracture planes. Through tensile experiments, it was revealed that, compared with the M-C criterion, the ellipse criterion presents a better prediction for the tensile fracture behavior of the investigated Zr-based MG in a wide normal stress range.

It is noted that the criteria mentioned above are mostly empirical or semiempirical, and the physical origin underlying these failure criteria is unclear. Moreover, for a full prediction of both tensile and compressive mechanical failure in MGs, a generalized criterion is urgently required. From the nature of short-range order in MGs, Chen et al. [14] built the connections between macroscopic failure and the unique atomic structure, and derived a unified failure criterion as:

$$(\sigma/\overline{\sigma}_0+\beta_{SD})^2+(\tau/(\alpha\overline{\sigma}_0))^2=1, \tag{2}$$

which involves three critical factors: The shear-to-normal strength ratio $\alpha=\tau_0/\overline{\sigma}_0$, the S-D factor β_{SD}, and the generalized normal strength $\overline{\sigma}_0$. The failure criterion geometrically constructs the eccentric ellipse-like failure envelope in the τ-σ stress space, as displayed by Fig. 21. Distinct failure modes correspond to ellipses of different shapes depending on α and β_{SD}. Figure 21a denotes shear failure with $45°<\theta^T<90°$ and $0°<\theta^C<45°$, while Fig. 21b represents normal tensile fracture with $\theta^T=90°$ and $\sigma^T=\sigma^T_{max}$. Based on the failure criterion, a failure map (Fig. 22) was further developed. In the map, the diverse failure modes (i.e., shear failure (I) and normal tensile fracture (II) in tension and shear failure (III) and splitting (IV) in compression) can be well unified. It also predicts the asymmetrical deviation of failure angles from 45° under uniaxial tension and compression. The transition from ductile failure to ideally brittle failure is revealed to be controlled by both factors α and β_{SD}.

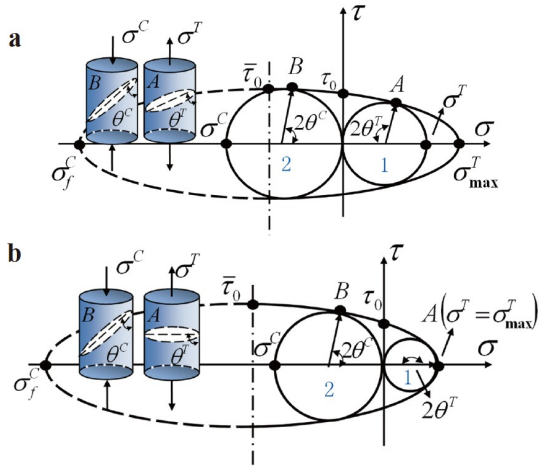

Figure 21 Eccentric ellipse-like failure envelope in the τ-σ stress space: **a** shear failure with $45°<\theta^T<90°$ and $0°<\theta^C<45°$ and **b** normal tensile fracture with $\theta^T=90°$ [14].

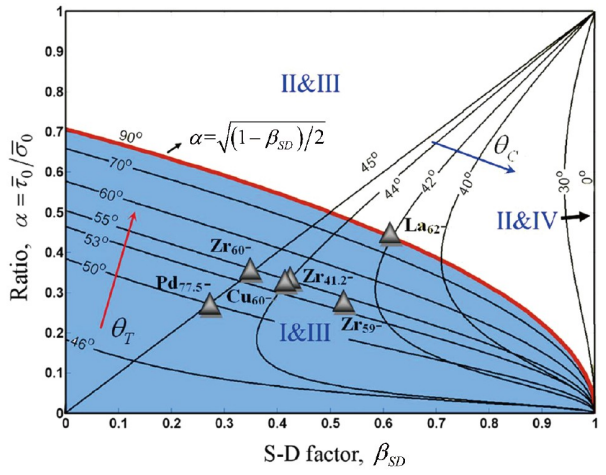

Figure 22 Tensile and compressive failure angles varying with the factors α and β_{SD} [14].

Based on the unified tensile fracture criterion, Qu and Zhang [54] considered the effect of external conditions and developed a more general fracture criterion that can be expressed by

$$\tau^2+\bar{\alpha}^2\hat{\beta}\sigma^2=\tau_0^2, \tag{3}$$

where $\hat{\beta}$ is an extrinsic parameter characterizing the effect of external loading. This criterion can be used for various external loading cases, and it is reduced to Eq. (1) when $\hat{\beta}=1$. Thereafter, regarding the material's failure as an energetic competition between shear and cleavage, a "generalized energy criterion" was proposed, and it was verified to be effective in predicting the tensile failure of MGs [206].

Song et al. [207] studied the torsional properties of Zr-based MGs. By comparing the experimental results with predictions from those classical criteria (i.e., Tresca, Mohr-Coulomb, and von Mises) and the newly developed ellipse and eccentric ellipse criteria [14,52], they proposed that the ellipse and eccentric ellipse criteria are more appropriate in describing the yield behavior of Zr-based MGs. The eccentric ellipse criteria first raised in MGs [14] were extended to amorphous materials and found to be essential for the tensile-shear failure of amorphous materials [208].

6. Closing remarks

The present review has summarized the current advances of the failure behavior and criteria in MGs. Although there have been a good number of studies on the failure of MGs, many problems still remain to be resolved and further clarified. Some of the outstanding issues in this connection that need to be investigated are listed below.

Although the onset conditions for shear banding or cavitation have been established, a general criterion to predict what kinds of instability modes occur is still absent. The inherent correlations between the atomic structure and these distinct instability modes remain elusive.

Shear band is regarded as a precursor of crack. However, convincing experimental evidence is still lacking on how a crack initiates from a shear band. To address this critical issue, more advanced experimental techniques are expected to obtain details on the spatial and temporal evolution of the shear band, the nucleation of nanovoids within the shear band, and the onset of microcracking.

The correlations of Poisson's ratio, pressure sensitivity and dilatancy factors with fracture toughness and ductility have been broadly revealed experimentally and theoretically, but the physical meaning and atomic basis for these governing parameters have not yet been clarified. The inherent relations among these parameters and their coupling effects on deformation and fracture need further study to explain the complex failure phenomena in MGs.

The crack tip field is a core problem in the study of solid fractures. The stress and strain distribution and plastic zone ahead of the crack tip determine the microfailure modes and induce distinct morphologies of the fracture surface. To date, a major understanding of the crack tip field of MGs comes from simulation and theoretical analysis, and only a few experimental works have derived limited information on the crack tip field. Delicate experiments satisfying the demand of spatial and temporal scales of crack tip fields in MGs are required to capture the evolution of the plastic zone, shear banding or cavitation ahead of the crack tip for both ductile and brittle failure to provide direct clues for different micromechanisms.

Crack instability and branching are the fundamental energy dissipation processes during dynamic fracture. For MGs of different toughness and ductility, their cracking behavior shows quite different traits, which are governed by the competition between the creation of a new fracture surface and the localized plastic flow ahead of the crack tip. Effective criteria need to be established to predict crack initiation, propagation and branching based on a clear physical picture of cracking.

This work was supported by the National Natural Science Foundation Basic Science Center Program for "Multiscale Problems in Nonlinear Mechanics" (Grant No. 11988102), the National Natural Science Foundation of China (Grant Nos. 11972346 and 11790292), the National Key Research and Development Program of China (Grant No. 2017YFB0702003), the Strategic Priority Research Program (Grant Nos. XDB22040302 and XDB22040303), the Key Research Program of Frontier Sciences (Grant No. QYZDJSSW-JSC011), and the Science Challenge Project (Grant No. TZ2018001).

1 F. Spaepen, A microscopic mechanism for steady state inhomogeneous flow in metallic glasses, Acta Metall. **25**, 407 (1977).
2 A. S. Argon, Plastic deformation in metallic glasses, Acta Metall. **27**, 47 (1979).
3 M. L. Falk, and J. S. Langer, Dynamics of viscoplastic deformation

in amorphous solids, Phys. Rev. E **57**, 7192 (1998).
4 G. Biroli, In search of the perfect glass, Nat. Phys. **10**, 555 (2014).
5 C. P. Goodrich, A. J. Liu, and S. R. Nagel, Solids between the mechanical extremes of order and disorder, Nat. Phys. **10**, 578 (2014).
6 D. B. Miracle, A structural model for metallic glasses, Nat. Mater. **3**, 697 (2004).
7 M. L. Falk, and J. S. Langer, Deformation and failure of amorphous, solidlike materials, Annu. Rev. Condens. Matter Phys. **2**, 353 (2011).
8 K. Kamrin, and E. Bouchbinder, Two-temperature continuum thermomechanics of deforming amorphous solids, J. Mech. Phys. Solids **73**, 269 (2014).
9 F. Spaepen, On the fracture morphology of metallic glasses, Acta Metall. **23**, 615 (1975).
10 A. S. Argon, and M. Salama, The mechanism of Fracture in Glassy materials capable of some inelastic deformation, Mater. Sci. Eng. **23**, 219 (1976).
11 C. Schuh, T. Hufnagel, and U. Ramamurty, Mechanical behavior of amorphous alloys, Acta Mater. **55**, 4067 (2007).
12 A. L. Greer, Y. Q. Cheng, and E. Ma, Shear bands in metallic glasses, Mater. Sci. Eng.-R-Rep. **74**, 71 (2013).
13 R. Raghavan, P. Murali, and U. Ramamurty, On factors influencing the ductile-to-brittle transition in a bulk metallic glass, Acta Mater. **57**, 3332 (2009).
14 Y. Chen, M. Q. Jiang, Y. J. Wei, and L. H. Dai, Failure criterion for metallic glasses, Philos. Mag. **91**, 4536 (2011).
15 M. Q. Jiang, Z. Ling, J. X. Meng, and L. H. Dai, Energy dissipation in fracture of bulk metallic glasses via inherent competition between local softening and quasi-cleavage, Philos. Mag. **88**, 407 (2008).
16 G. Ravichandran, and A. Molinari, Analysis of shear banding in metallic glasses under bending, Acta Mater. **53**, 4087 (2005).
17 J. Xu, U. Ramamurty, and E. Ma, The fracture toughness of bulk metallic glasses, JOM **62**, 10 (2010).
18 R. L. Narayan, P. Tandaiya, R. Narasimhan, and U. Ramamurty, Wallner lines, crack velocity and mechanisms of crack nucleation and growth in a brittle bulk metallic glass, Acta Mater. **80**, 407 (2014).
19 P. Tandaiya, U. Ramamurty, and R. Narasimhan, Mixed mode (I and II) crack tip fields in bulk metallic glasses, J. Mech. Phys. Solids **57**, 1880 (2009).
20 P. Tandaiya, R. Narasimhan, and U. Ramamurty, On the mechanism and the length scales involved in the ductile fracture of a bulk metallic glass, Acta Mater. **61**, 1558 (2013).
21 R. Narasimhan, P. Tandaiya, I. Singh, R. L. Narayan, and U. Ramamurty, Fracture in metallic glasses: Mechanics and mechanisms, Int. J. Fract. **191**, 53 (2015).
22 D. Jang, C. T. Gross, and J. R. Greer, Effects of size on the strength and deformation mechanism in Zr-based metallic glasses, Int. J. Plast. **27**, 858 (2011).
23 K. M. Flores, and R. H. Dauskardt, Mean stress effects on flow localization and failure in a bulk metallic glass, Acta Mater. **49**, 2527 (2001).
24 J. W. Rudnicki, and J. R. Rice, Conditions for the localization of deformation in pressure-sensitive dilatant materials, J. Mech. Phys. Solids **23**, 371 (1975).
25 F. Z. Li, and J. Pan, Plane-strain crack-tip fields for pressure-sensitive dilatant materials, J. Appl. Mech. **57**, 40 (1990).
26 F. Z. Li, and J. Pan, Plane-stress crack-tip fields for pressure-sensitive dilatant materials, Eng. Fract. Mech. **35**, 1105 (1990).
27 H. Guo, P. F. Yan, Y. B. Wang, J. Tan, Z. F. Zhang, M. L. Sui, and E. Ma, Tensile ductility and necking of metallic glass, Nat. Mater. **6**, 735 (2007).
28 L. H. Dai, M. Yan, L. F. Liu, and Y. L. Bai, Adiabatic shear banding instability in bulk metallic glasses, Appl. Phys. Lett. **87**, 141916 (2005).
29 Y. Chen, M. Q. Jiang, and L. H. Dai, Collective evolution dynamics of multiple shear bands in bulk metallic glasses, Int. J. Plast. **50**, 18 (2013).
30 W. Jiang, G. Fan, F. Liu, G. Wang, H. Choo, and P. Liaw, Spatio-temporally inhomogeneous plastic flow of a bulk-metallic glass, Int. J. Plast. **24**, 1 (2008).
31 K. W. Chen, and J. F. Lin, Investigation of the relationship between primary and secondary shear bands induced by indentation in bulk metallic glasses, Int. J. Plast. **26**, 1645 (2010).
32 I. Singh, T. F. Guo, P. Murali, R. Narasimhan, Y. W. Zhang, and H. J. Gao, Cavitation in materials with distributed weak zones: Implications on the origin of brittle fracture in metallic glasses, J. Mech. Phys. Solids **61**, 1047 (2013).
33 P. Murali, T. F. Guo, Y. W. Zhang, R. Narasimhan, Y. Li, and H. J. Gao, Atomic scale fluctuations govern brittle fracture and cavitation behavior in metallic glasses, Phys. Rev. Lett. **107**, 215501 (2011).
34 I. Singh, T. F. Guo, R. Narasimhan, and Y. W. Zhang, Cavitation in brittle metallic glasses—Effects of stress state and distributed weak zones, Int. J. Solids Struct. **51**, 4373 (2014).
35 B. A. Sun, and W. H. Wang, The fracture of bulk metallic glasses, Prog. Mater. Sci. **74**, 211 (2015).
36 X. Huang, Z. Ling, and L. H. Dai, Ductile-to-brittle transition in spallation of metallic glasses, J. Appl. Phys. **116**, 143503 (2014).
37 M. Q. Jiang, and L. H. Dai, On the origin of shear banding instability in metallic glasses, J. Mech. Phys. Solids **57**, 1267 (2009).
38 D. Klaumünzer, R. Maaß, and J. F. Löffler, Stick-slip dynamics and recent insights into shear banding in metallic glasses, J. Mater. Res. **26**, 1453 (2011).
39 R. Maaß, D. Klaumünzer, and J. F. Löffler, Propagation dynamics of individual shear bands during inhomogeneous flow in a Zr-based bulk metallic glass, Acta Mater. **59**, 3205 (2011).
40 S. X. Song, H. Bei, J. Wadsworth, and T. G. Nieh, Flow serration in a Zr-based bulk metallic glass in compression at low strain rates, Intermetallics **16**, 813 (2008).
41 S. X. Song, and T. G. Nieh, Flow serration and shear-band viscosity during inhomogeneous deformation of a Zr-based bulk metallic glass, Intermetallics **17**, 762 (2009).
42 Y. Q. Cheng, Z. Han, Y. Li, and E. Ma, Cold versus hot shear banding in bulk metallic glass, Phys. Rev. B **80**, 134115 (2009).
43 Z. Han, W. F. Wu, Y. Li, Y. J. Wei, and H. J. Gao, An instability index of shear band for plasticity in metallic glasses, Acta Mater. **57**, 1367 (2009).
44 L. F. Liu, L. H. Dai, Y. L. Bai, and B. C. Wei, Initiation and propagation of shear bands in Zr-based bulk metallic glass under quasi-static and dynamic shear loadings, J. Non-Crystal. Solids **351**, 3259 (2005).
45 M. Q. Jiang, and L. H. Dai, Shear-band toughness of bulk metallic glasses, Acta Mater. **59**, 4525 (2011).
46 Y. Chen, and L. H. Dai, Nature of crack-tip plastic zone in metallic glasses, Int. J. Plast. **77**, 54 (2016).
47 K. M. Flores, and R. H. Dauskardt, Mode II fracture behavior of a Zr-based bulk metallic glass, J. Mech. Phys. Solids **54**, 2418 (2006).
48 P. Tandaiya, R. Narasimhan, and U. Ramamurty, Mode I crack tip fields in amorphous materials with application to metallic glasses, Acta Mater. **55**, 6541 (2007).
49 P. Tandaiya, U. Ramamurty, G. Ravichandran, and R. Narasimhan, Effect of Poisson's ratio on crack tip fields and fracture behavior of metallic glasses, Acta Mater. **56**, 6077 (2008).
50 J. J. Lewandowski, W. H. Wang, and A. L. Greer, Intrinsic plasticity or brittleness of metallic glasses, Philos. Mag. Lett. **85**, 77 (2005).
51 J. Schroers, and W. L. Johnson, Ductile bulk metallic glass, Phys. Rev. Lett. **93**, 255506 (2004).
52 Z. F. Zhang, and J. Eckert, Unified tensile fracture criterion, Phys. Rev. Lett. **94**, 094301 (2005).
53 R. T. Qu, J. Eckert, and Z. F. Zhang, Tensile fracture criterion of metallic glass, J. Appl. Phys. **109**, 083544 (2011).
54 R. T. Qu, and Z. F. Zhang, A universal fracture criterion for high-strength materials, Sci. Rep. **3**, 1117 (2013).
55 J. Xu, and E. Ma, Damage-tolerant Zr-Cu-Al-based bulk metallic glasses with record-breaking fracture toughness, J. Mater. Res. **29**,

1489 (2014).
56 M. D. Demetriou, M. E. Launey, G. Garrett, J. P. Schramm, D. C. Hofmann, W. L. Johnson, and R. O. Ritchie, A damage-tolerant glass, Nat. Mater. **10**, 123 (2011).
57 Y. H. Liu, G. Wang, R. J. Wang, D. Q. Zhao, M. X. Pan, and W. H. Wang, Super plastic bulk metallic glasses at room temperature, Science **315**, 1385 (2007).
58 J. Pan, Y. P. Ivanov, W. H. Zhou, Y. Li, and A. L. Greer, Strain-hardening and suppression of shear-banding in rejuvenated bulk metallic glass, Nature **578**, 559 (2020).
59 Y. Liu, T. H. Zhang, B. C. Wei, D. M. Xing, W. H. Li, and L. C. Zhang, Effect of structural relaxation on deformation behaviour of Zr-based metallic glass, Chin. Phys. Lett. **23**, 1868 (2006).
60 J. Das, K. B. Kim, W. Xu, B. C. Wei, Z. F. Zhang, W. H. Wang, S. Yi, and J. Eckert, Ductile metallic glasses in supercooled martensitic alloys, Mater. Trans. **47**, 2606 (2006).
61 T. Wang, J. Si, Y. Wu, K. Lv, Y. Liu, and X. Hui, Two-step work-hardening and its gigantic toughening effect in Zr-based bulk metallic glasses, Script. Mater. **150**, 106 (2018).
62 L. F. Liu, L. H. Dai, Y. L. Bai, B. C. Wei, and J. Eckert, Behavior of multiple shear bands in Zr-based bulk metallic glass, Mater. Chem. Phys. **93**, 174 (2005).
63 Z. F. Zhang, H. Zhang, X. F. Pan, J. Das, and J. Eckert, Effect of aspect ratio on the compressive deformation and fracture behaviour of Zr-based bulk metallic glass, Philos. Mag. Lett. **85**, 513 (2005).
64 C. A. Schuh, and A. C. Lund, Atomistic basis for the plastic yield criterion of metallic glass, Nat. Mater. **2**, 449 (2003).
65 C. H. Hsueh, H. Bei, C. T. Liu, P. F. Becher, and E. P. George, Shear fracture of bulk metallic glasses with controlled applied normal stresses, Script. Mater. **59**, 111 (2008).
66 V. Keryvin, Indentation as a probe for pressure sensitivity of metallic glasses, J. Phys.-Condens. Matter **20**, 114119 (2008).
67 G. C. Rauch, and W. C. Leslie, The extent and nature of the strength-differential effect in steels, Metall. Trans. **3**, 377 (1972).
68 H. Altenbach, G. B. Stoychev, and K. N. Tushtev, On elastoplastic deformation of grey cast iron, Int. J. Plast. **17**, 719 (2001).
69 J. P. Hirth, M. Cohen, On the strength-Differential Phenomenon in Hardened steel, Metall. Trans. **1**, 6 (1970).
70 D. C. Drucker, Plasticity theory strength-differential (SD) phenomenon, and volume expansion in metals and plastics, Metall. Trans. **4**, 667 (1973).
71 L. A. Davis, and S. Kavesh, Deformation and fracture of an amorphous metallic alloy at high pressure, J Mater Sci **10**, 453 (1975).
72 H. Kimura, T. Masumoto, Amorphous metallic alloys, in: F. E. Luborsky, ed. Amorphous Metallic Alloys, (Butterworths Co., London, 1983).
73 P. E. Donovan, A yield criterion for $Pd_{40}Ni_{40}P_{20}$ metallic glass, Acta Metall. **37**, 445 (1989).
74 T. Mukai, T. G. Nieh, Y. Kawamura, A. Inoue, and K. Higashi, Effect of strain rate on compressive behavior of a $Pd_{40}Ni_{40}P_{20}$ bulk metallic glass, Intermetallics **10**, 1071 (2002).
75 T. Mukai, T. G. Nieh, Y. Kawamura, A. Inoue, and K. Higashi, Dynamic response of a $Pd_{40}Ni_{40}P_{20}$ bulk metallic glass in tension, Script. Mater. **46**, 43 (2002).
76 J. J. Lewandowski, and P. Lowhaphandu, Effects of hydrostatic pressure on the flow and fracture of a bulk amorphous metal, Philos. Mag. A **82**, 3427 (2002).
77 A. V. Sergueeva, N. A. Mara, J. D. Kuntz, E. J. Lavernia, and A. K. Mukherjee, Shear band formation and ductility in bulk metallic glass, Philos. Mag. **85**, 2671 (2005).
78 H. A. Bruck, T. Christman, A. J. Rosakis, and W. L. Johnson, Quasi-static constitutive behavior of $Zr_{41.25}Ti_{13.75}Ni_{10}Cu_{12.5}Be_{22.5}$ bulk amorphous alloys, Script. Metall. Mater. **30**, 429 (1994).
79 C. T. Liu, L. Heatherly, J. A. Horton, D. S. Easton, C. A. Carmichael, J. L. Wright, J. H. Schneibel, M. H. Yoo, C. H. Chen, and A. Inoue, Test environments and mechanical properties of Zr-base bulk amorphous alloys, Metall. Mat. Trans. A **29**, 1811 (1998).
80 G. He, J. Lu, Z. Bian, D. Chen, G. Chen, G. Tu, and G. Chen, Fracture morphology and quenched-in precipitates induced embrittlement in a Zr-base bulk glass, Mater. Trans. **42**, 356 (2001).
81 Z. F. Zhang, J. Eckert, and L. Schultz, Fatigue and fracture behavior of bulk metallic glass, Metall. Mat. Trans. A **35**, 3489 (2004).
82 T. Yoshikawa, M. Tokuda, and T. Inaba, Influence of thermoplastic deformation on mechanical properties of Zr-based bulk metallic glasses at room temperature, Int. J. Mech. Sci. **50**, 888 (2008).
83 V. Keryvin, M. L. Vaillant, T. Rouxel, M. Huger, T. Gloriant, and Y. Kawamura, Thermal stability and crystallisation of a $Zr_{55}Cu_{30}Al_{10}Ni_5$ bulk metallic glass studied by *in situ* ultrasonic echography, Intermetallics **10**, 1289 (2002).
84 T. Hirano, H. Kato, A. Matsuo, Y. Kawamura, and A. Inoue, Synthesis and mechanical properties of $Zr_{55}Al_{10}Ni_5Cu_{30}$ bulk glass composites containing ZrC particles formed by the *in-situ* reaction, Mater. Trans. JIM **41**, 1454 (2000).
85 F. Szuecs, C. P. Kim, and W. L. Johnson, Mechanical properties of $Zr_{56.2}Ti_{13.8}Nb_{5.0}Cu_{6.9}Ni_{5.6}Be_{12.5}$ ductile phase reinforced bulk metallic glass composite, Acta Mater. **49**, 1507 (2001).
86 R. D. Conner, Y. Li, W. D. Nix, and W. L. Johnson, Shear band spacing under bending of Zr-based metallic glass plates, Acta Mater. **52**, 2429 (2004).
87 Z. F. Zhang, J. Eckert, and L. Schultz, Difference in compressive and tensile fracture mechanisms of $Zr_{59}Cu_{20}Al_{10}Ni_8Ti_3$ bulk metallic glass, Acta Mater. **51**, 1167 (2003).
88 A. Inoue, Stabilization of metallic supercooled liquid and bulk amorphous alloys, Acta Mater. **48**, 279 (2000).
89 A. Inoue, W. Zhang, T. Zhang, and K. Kurosaka, High-strength Cu-based bulk glassy alloys in Cu-Zr-Ti and Cu-Hf-Ti ternary systems, Acta Mater. **49**, 2645 (2001).
90 T. Masumoto, and R. Maddin, The mechanical properties of palladium 20 a/o silicon alloy quenched from the liquid state, Acta Metall. **19**, 725 (1971).
91 A. Inoue, S. Sobu, D. V. Louzguine, H. Kimura, and K. Sasamori, Ultrahigh strength al-based amorphous alloys containing Sc, J. Mater. Res. **19**, 1539 (2004).
92 M. L. Lee, Y. Li, and C. A. Schuh, Effect of a controlled volume fraction of dendritic phases on tensile and compressive ductility in La-based metallic glass matrix composites, Acta Mater. **52**, 4121 (2004).
93 Z. F. Zhang, G. He, J. Eckert, and L. Schultz, Fracture Mechanisms in bulk metallic glassy materials, Phys. Rev. Lett. **91**, 045505 (2003).
94 J. Saida, and A. Inoue, Microstructure of tensile fracture in nanoicosahedral quasicrystal dispersed $Zr_{80}Pt_{20}$ amorphous alloy, Script. Mater. **50**, 1297 (2004).
95 M. Stoica, J. Eckert, S. Roth, Z. F. Zhang, L. Schultz, and W. H. Wang, Mechanical behavior of $Fe_{65.5}Cr_4Mo_4Ga_4P_{12}C_5B_{5.5}$ bulk metallic glass, Intermetallics **13**, 764 (2005).
96 Q. He, J. K. Shang, E. Ma, and J. Xu, Crack-resistance curve of a Zr–Ti-Cu–Al bulk metallic glass with extraordinary fracture toughness, Acta Mater. **60**, 4940 (2012).
97 X. K. Xi, D. Q. Zhao, M. X. Pan, W. H. Wang, Y. Wu, and J. J. Lewandowski, Fracture of brittle metallic glasses: Brittleness or plasticity, Phys. Rev. Lett. **94**, 125510 (2005).
98 G. Wang, Y. T. Wang, Y. H. Liu, M. X. Pan, D. Q. Zhao, and W. H. Wang, Evolution of nanoscale morphology on fracture surface of brittle metallic glass, Appl. Phys. Lett. **89**, 121909 (2006).
99 R. O. Ritchie, The conflicts between strength and toughness, Nat. Mater. **10**, 817 (2011).
100 F. F. Wu, W. Zheng, S. D. Wu, Z. F. Zhang, and J. Shen, Shear stability of metallic glasses, Int. J. Plast. **27**, 560 (2011).
101 C. Fan, H. Li, L. J. Kecskes, K. Tao, H. Choo, P. K. Liaw, and C. T. Liu, Mechanical behavior of bulk amorphous alloys reinforced by ductile particles at cryogenic temperatures, Phys. Rev. Lett. **96**, 145506 (2006).
102 J. X. Meng, Z. Ling, M. Q. Jiang, H. S. Zhang, and L. H. Dai, Dynamic fracture instability of tough bulk metallic glass, Appl. Phys.

Lett. **92**, 171909 (2008).
103 J. P. Escobedo, and Y. M. Gupta, Dynamic tensile response of Zr-based bulk amorphous alloys: Fracture morphologies and mechanisms, J. Appl. Phys. **107**, 123502 (2010).
104 Z. F. Zhang, F. F. Wu, W. Gao, J. Tan, Z. G. Wang, M. Stoica, J. Das, J. Eckert, B. L. Shen, and A. Inoue, Wavy cleavage fracture of bulk metallic glass, Appl. Phys. Lett. **89**, 251917 (2006).
105 M. Q. Jiang, J. X. Meng, J. B. Gao, X. L. Wang, T. Rouxel, V. Keryvin, Z. Ling, and L. H. Dai, Fractal in fracture of bulk metallic glass, Intermetallics **18**, 2468 (2010).
106 G. Wang, D. Q. Zhao, H. Y. Bai, M. X. Pan, A. L. Xia, B. S. Han, X. K. Xi, Y. Wu, and W. H. Wang, Nanoscale periodic morphologies on the fracture surface of brittle metallic glasses, Phys. Rev. Lett. **98**, 235501 (2007).
107 X. K. Xi, D. Q. Zhao, M. X. Pan, W. H. Wang, Y. Wu, and J. J. Lewandowski, Periodic corrugation on dynamic fracture surface in brittle bulk metallic glass, Appl. Phys. Lett. **89**, 181911 (2006).
108 R. Huang, Z. Suo, J. H. Prevost, and W. D. Nix, Inhomogeneous deformation in metallic glasses, J. Mech. Phys. Solids **50**, 1011 (2002).
109 G. Subhash, and H. Zhang, Shear band patterns in metallic glasses under static indentation, dynamic indentation, and scratch processes, Metall. Mat. Trans. A **38**, 2936 (2007).
110 P. S. Steif, F. Spaepen, and J. W. Hutchinson, Strain localization in amorphous metals, Acta Metall. **30**, 447 (1982).
111 B. Yang, M. L. Morrison, P. K. Liaw, R. A. Buchanan, G. Wang, C. T. Liu, and M. Denda, Dynamic evolution of nanoscale shear bands in a bulk-metallic glass, Appl. Phys. Lett. **86**, 141904 (2005).
112 L. H. Dai, Shear banding in bulk metallic glasses, in: B. Dodd, Y. L. Bai, Eds. Adiabatic Shear Localization: Frontiers and Advances (Elsevier, London, 2012), pp. 311–361.
113 J. W. Cui, R. T. Qu, F. F. Wu, Z. F. Zhang, B. L. Shen, M. Stoica, and J. Eckert, Shear band evolution during large plastic deformation of brittle and ductile metallic glasses, Philos. Mag. Lett. **90**, 573 (2010).
114 U. Ramamurty, S. Jana, Y. Kawamura, and K. Chattopadhyay, Hardness and plastic deformation in a bulk metallic glass, Acta Mater. **53**, 705 (2005).
115 W. L. Johnson, and K. Samwer, A universal criterion for plastic yielding of metallic glasses with a $(T/Tg)^{2/3}$ temperature dependence, Phys. Rev. Lett. **95**, 195501 (2005).
116 L. Sun, M. Q. Jiang, and L. H. Dai, Intrinsic correlation between dilatation and pressure sensitivity of plastic flow in metallic glasses, Script. Mater. **63**, 945 (2010).
117 B. A. Sun, H. B. Yu, W. Jiao, H. Y. Bai, D. Q. Zhao, and W. H. Wang, Plasticity of ductile metallic glasses: A self-organized critical state, Phys. Rev. Lett. **105**, 035501 (2010).
118 F. Spaepen, Defects in amorphous metals, in: R. Balian, et al. eds. Les Houches Lectures XXXV on Physics of Defects, (North-Holland, Amsterdam, 1981), pp. 133–174.
119 P. Zhao, J. Li, and Y. Wang, Heterogeneously randomized STZ model of metallic glasses: Softening and extreme value statistics during deformation, Int. J. Plast. **40**, 1 (2013).
120 M. Chen, Mechanical behavior of metallic glasses: Microscopic understanding of strength and ductility, Annu. Rev. Mater. Res. **38**, 445 (2008).
121 W. H. Wang, The elastic properties, elastic models and elastic perspectives of metallic glasses, Prog. Mater. Sci. **57**, 487 (2012).
122 D. Pan, A. Inoue, T. Sakurai, and M. W. Chen, Experimental characterization of shear transformation zones for plastic flow of bulk metallic glasses, Proc. Natl. Acad. Sci. USA **105**, 14769 (2008).
123 C. Maloney, and A. Lemaître, Subextensive scaling in the athermal, quasistatic limit of amorphous matter in plastic shear flow, Phys. Rev. Lett. **93**, 016001 (2004).
124 A. Lemaître, and C. Caroli, Rate-dependent avalanche size in athermally sheared amorphous solids, Phys. Rev. Lett. **103**, 065501 (2009).
125 F. Jiang, M. Q. Jiang, H. F. Wang, Y. L. Zhao, L. He, and J. Sun, Shear transformation zone volume determining ductile-brittle transition of bulk metallic glasses, Acta Mater. **59**, 2057 (2011).
126 D. Pan, Y. Yokoyama, T. Fujita, Y. H. Liu, S. Kohara, A. Inoue, and M. W. Chen, Correlation between structural relaxation and shear transformation zone volume of a bulk metallic glass, Appl. Phys. Lett. **95**, 141909 (2009).
127 D. Şopu, A. Stukowski, M. Stoica, and S. Scudino, Atomic-level processes of shear band nucleation in metallic glasses, Phys. Rev. Lett. **119**, 195503 (2017).
128 Z. L. Tian, Y. J. Wang, Y. Chen, and L. H. Dai, Strain gradient drives shear banding in metallic glasses, Phys. Rev. B **96**, 094103 (2017).
129 H. J. Leamy, T. T. Wang, and H. S. Chen, Plastic flow and fracture of metallic glass, Metall. Trans. **3**, 699 (1972).
130 W. J. Wright, R. B. Schwarz, and W. D. Nix, Localized heating during serrated plastic flow in bulk metallic glasses, Mater. Sci. Eng.-A **319-321**, 229 (2001).
131 C. A. Pampillo, and H. S. Chen, Comprehensive plastic deformation of a bulk metallic glass, Mater. Sci. Eng. **13**, 181 (1974).
132 L. H. Dai, and Y. L. Bai, Basic mechanical behaviors and mechanics of shear banding in BMGs, Int. J. Impact Eng. **35**, 704 (2008).
133 Q. Yang, A. Mota, and M. Ortiz, A finite-deformation constitutive model of bulk metallic glass plasticity, Comput. Mech. **37**, 194 (2006).
134 P. Thamburaja, and R. Ekambaram, Coupled thermo-mechanical modelling of bulk-metallic glasses: Theory, finite-element simulations and experimental verification, J. Mech. Phys. Solids **55**, 1236 (2007).
135 D. D. E. Brennhaugen, K. Georgarakis, Y. Yokoyama, K. S. Nakayama, L. Arnberg, and R. E. Aune, Probing heat generation during tensile plastic deformation of a bulk metallic glass at cryogenic temperature, Sci. Rep. **8**, 16317 (2018).
136 J. Fornell, A. Concustell, S. Suriñach, W. H. Li, N. Cuadrado, A. Gebert, M. D. Baró, and J. Sort, Yielding and intrinsic plasticity of Ti-Zr-Ni-Cu-Be bulk metallic glass, Int. J. Plast. **25**, 1540 (2009).
137 R. T. Ott, F. Sansoz, T. Jiao, D. Warner, J. F. Molinari, K. T. Ramesh, T. C. Hufnagel, and C. Fan, Yield criteria and strain-rate behavior of $Zr_{57.4}Cu_{16.4}Ni_{8.2}Ta_8Al_{10}$ metallic-glass-matrix composites, Metall. Mat. Trans. A **37**, 3251 (2006).
138 Y. F. Gao, L. Wang, H. Bei, and T. G. Nieh, On the shear-band direction in metallic glasses, Acta Mater. **59**, 4159 (2011).
139 H. H. Ruan, L. C. Zhang, and J. Lu, A new constitutive model for shear banding instability in metallic glass, Int. J. Solids Struct. **48**, 3112 (2011).
140 Y. Chen, and L. Dai, Onset and direction of shear banding instability in metallic glasses, J. Mater. Sci. Tech. **30**, 616 (2014).
141 H. Neuhäuser, Rate of shear band formation in metallic glasses, Script. Metall. **12**, 471 (1978).
142 W. J. Wright, M. W. Samale, T. C. Hufnagel, M. M. LeBlanc, and J. N. Florando, Studies of shear band velocity using spatially and temporally resolved measurements of strain during quasistatic compression of a bulk metallic glass, Acta Mater. **57**, 4639 (2009).
143 A. Vinogradov, On shear band velocity and the detectability of acoustic emission in metallic glasses, Script. Mater. **63**, 89 (2010).
144 S. Y. Jiang, M. Q. Jiang, L. H. Dai, and Y. G. Yao, Atomistic origin of rate-dependent serrated plastic flow in metallic glasses, Nanoscale Res. Lett. **3**, 524 (2008).
145 R. D. Conner, W. L. Johnson, N. E. Paton, and W. D. Nix, Shear bands and cracking of metallic glass plates in bending, J. Appl. Phys. **94**, 904 (2003).
146 D. B. Miracle, A. Concustell, Y. Zhang, A. R. Yavari, and A. L. Greer, Shear bands in metallic glasses: Size effects on thermal profiles, Acta Mater. **59**, 2831 (2011).
147 H. Zhang, S. Maiti, and G. Subhash, Evolution of shear bands in bulk metallic glasses under dynamic loading, J. Mech. Phys. Solids **56**, 2171 (2008).
148 D. C. Hofmann, J. Y. Suh, A. Wiest, G. Duan, M. L. Lind, M. D. Demetriou, and W. L. Johnson, Designing metallic glass matrix

composites with high toughness and tensile ductility, Nature **451**, 1085 (2008).
149 J. Das, M. B. Tang, K. B. Kim, R. Theissmann, F. Baier, W. H. Wang, and J. Eckert, "Work-Hardenable" ductile bulk metallic glass, Phys. Rev. Lett. **94**, 205501 (2005).
150 K. F. Yao, F. Ruan, Y. Q. Yang, and N. Chen, Superductile bulk metallic glass, Appl. Phys. Lett. **88**, 122106 (2006).
151 L. Y. Chen, Z. D. Fu, G. Q. Zhang, X. P. Hao, Q. K. Jiang, X. D. Wang, Q. P. Cao, H. Franz, Y. G. Liu, H. S. Xie, S. L. Zhang, B. Y. Wang, Y. W. Zeng, and J. Z. Jiang, New class of plastic bulk metallic glass, Phys. Rev. Lett. **100**, 075501 (2008).
152 C. C. Hays, C. P. Kim, and W. L. Johnson, Microstructure controlled shear band pattern formation and enhanced plasticity of bulk metallic glasses containing *in situ* formed ductile phase dendrite dispersions, Phys. Rev. Lett. **84**, 2901 (2000).
153 Y. Chen, M. Q. Jiang, and L. H. Dai, How does the initial free volume distribution affect shear band formation in metallic glass? Sci. China-Phys. Mech. Astron. **54**, 1488 (2011).
154 X. Hui, S. N. Liu, S. J. Pang, L. C. Zhuo, T. Zhang, G. L. Chen, and Z. K. Liu, High-zirconium-based bulk metallic glasses with large plasticity, Script. Mater. **63**, 239 (2010).
155 S. Xie, and E. P. George, Hardness and shear band evolution in bulk metallic glasses after plastic deformation and annealing, Acta Mater. **56**, 5202 (2008).
156 H. Zhang, X. Jing, G. Subhash, L. J. Kecskes, and R. J. Dowding, Investigation of shear band evolution in amorphous alloys beneath a Vickers indentation, Acta Mater. **53**, 3849 (2005).
157 A. Bharathula, S. W. Lee, W. J. Wright, and K. M. Flores, Compression testing of metallic glass at small length scales: Effects on deformation mode and stability, Acta Mater. **58**, 5789 (2010).
158 D. E. Grady, and M. E. Kipp, The growth of unstable thermoplastic shear with application to steady-wave shock compression in solids, J. Mech. Phys. Solids **35**, 95 (1987).
159 D. E. Grady, Properties of an adiabatic shear-band process zone, J. Mech. Phys. Solids **40**, 1197 (1992).
160 D. E. Grady, Adiabatic shear failure in brittle solids, Int. J. Impact Eng. **38**, 661 (2011).
161 T. W. Wright, and H. Ockendon, A scaling law for the effect of inertia on the formation of adiabatic shear bands, Int. J. Plast. **12**, 927 (1996).
162 Y. Wei, X. Lei, L. S. Huo, W. H. Wang, and A. L. Greer, Towards more uniform deformation in metallic glasses: The role of Poisson's ratio, Mater. Sci. Eng.-A **560**, 510 (2013).
163 B. G. Yoo, J. Y. Kim, Y. J. Kim, I. C. Choi, S. Shim, T. Y. Tsui, H. Bei, U. Ramamurty, and J. Jang, Increased time-dependent room temperature plasticity in metallic glass nanopillars and its size-dependency, Int. J. Plast. **37**, 108 (2012).
164 C. A. Volkert, A. Donohue, and F. Spaepen, Effect of sample size on deformation in amorphous metals, J. Appl. Phys. **103**, 083539 (2008).
165 J. R. Greer, and J. T. M. De Hosson, Plasticity in small-sized metallic systems: Intrinsic versus extrinsic size effect, Prog. Mater. Sci. **56**, 654 (2011).
166 G. Kumar, A. Desai, and J. Schroers, Bulk metallic glass: The smaller the better, Adv. Mater. **23**, 461 (2011).
167 D. Jang, and J. R. Greer, Transition from a strong-yet-brittle to a stronger-and-ductile state by size reduction of metallic glasses, Nat. Mater. **9**, 215 (2010).
168 X. Zhou, H. Zhou, X. Li, and C. Chen, Size effects on tensile and compressive strengths in metallic glass nanowires, J. Mech. Phys. Solids **84**, 130 (2015).
169 E. Bouchaud, D. Boivin, J. L. Pouchou, D. Bonamy, B. Poon, and G. Ravichandran, Fracture through cavitation in a metallic glass, Europhys. Lett. **83**, 66006 (2008).
170 R. F. Bishop, R. Hill, and N. F. Mott, The theory of indentation and hardness tests, Proc. Phys. Soc. **57**, 147 (1945).
171 P. Chadwick, The quasi-static expansion of a spherical cavity in metals and ideal soils, Q J Mech. Appl. Math. **12**, 52 (1959).
172 D. Durban, and M. Baruch, On the problem of a spherical cavity in an infinite elasto-plastic medium, J. Appl. Mech. **43**, 633 (1976).
173 Y. Huang, J. W. Hutchinson, and V. Tvergaard, Cavitation instabilities in elastic-plastic solids, J. Mech. Phys. Solids **39**, 223 (1991).
174 P. Murali, R. Narasimhan, T. F. Guo, Y. W. Zhang, and H. J. Gao, Shear bands mediate cavitation in brittle metallic glasses, Script. Mater. **68**, 567 (2013).
175 P. Guan, S. Lu, M. J. B. Spector, P. K. Valavala, and M. L. Falk, Cavitation in amorphous solids, Phys. Rev. Lett. **110**, 185502 (2013).
176 X. Huang, Z. Ling, Y. J. Wang, and L. H. Dai, Intrinsic structural defects on medium range in metallic glasses, Intermetallics **75**, 36 (2016).
177 L. Q. Shen, J. H. Yu, X. C. Tang, B. A. Sun, Y. H. Liu, H. Y. Bai, and W. H. Wang, Observation of cavitation governing fracture in glasses, Sci. Adv. **7**, eabf7293 (2021).
178 X. Huang, Z. Ling, H. S. Zhang, J. Ma, and L. H. Dai, How does spallation microdamage nucleate in bulk amorphous alloys under shock loading? J. Appl. Phys. **110**, 103519 (2011).
179 X. Huang, Z. Ling, and L. H. Dai, Cavitation instabilities in bulk metallic glasses, Int. J. Solids Struct. **50**, 1364 (2013).
180 X. Huang, Z. Ling, and L. H. Dai, Influence of surface energy and thermal effects on cavitation instabilities in metallic glasses, Mech. Mater. **131**, 113 (2019).
181 J. R. Rice, A path independent integral and the approximate analysis of strain concentration by notches and cracks, J. Appl. Mech. **35**, 379 (1968).
182 J. W. Hutchinson, Plastic stress and strain fields at a crack tip, J. Mech. Phys. Solids **16**, 337 (1968).
183 J. R. Rice, and G. F. Rosengren, Plane strain deformation near a crack tip in a power-law hardening material, J. Mech. Phys. Solids **16**, 1 (1968).
184 J. Pan, and C. F. Shih, Plane-stress crack-tip fields for power-law hardening orthotropic materials, Int. J. Fract. **37**, 171 (1988).
185 J. Pan, and C. F. Shih, Plane-strain crack-tip fields for power-law hardening orthotropic materials, Mech. Mater. **5**, 299 (1986).
186 J. W. Hutchinson, Constitutive behavior and crack tip fields for materials undergoing creep-constrained grain boundary cavitation, Acta Metall. **31**, 1079 (1983).
187 H. Gao, and J. R. Rice, Shear stress intensity factors for a planar crack with slightly curved front, J. Appl. Mech. **53**, 774 (1986).
188 N. R. F. Elfakhakhre, N. M. A. Nik Long, and Z. K. Eshkuvatov, Numerical solutions for cracks in an elastic half-plane, Acta Mech. Sin. **35**, 212 (2018).
189 X. Ji, and F. Zhu, Finite element simulation of elastoplastic field near crack tips and results for a central cracked plate of LE-LHP material under tension, Acta Mech. Sin. **35**, 828 (2019).
190 Z. E. Liu, and Y. Wei, An analytical solution to the stress fields of kinked cracks, J. Mech. Phys. Solids **156**, 104619 (2021).
191 H. Y. Jeong, X. W. Li, A. F. Yee, and J. Pan, Slip lines in front of a round notch tip in a pressure-sensitive material, Mech. Mater. **19**, 29 (1994).
192 S. Basu, and E. V. Giessen, A thermo-mechanical study of mode I, small-scale yielding crack-tip fields in glassy polymers, Int. J. Plast. **18**, 1395 (2002).
193 H. Y. Subramanya, S. Viswanath, and R. Narasimhan, A three-dimensional numerical study of mode I crack tip fields in pressure sensitive plastic solids, Int. J. Solids Struct. **44**, 1863 (2007).
194 P. Lowhaphandu, and J. J. Lewandowski, Fracture toughness and notched toughness of bulk amorphous alloy: Zr-Ti-Ni-Cu-Be, Script. Mater. **38**, 1811 (1998).
195 L. Anand, and C. Su, A theory for amorphous viscoplastic materials undergoing finite deformations, with application to metallic glasses, J. Mech. Phys. Solids **53**, 1362 (2005).
196 D. L. Henann, and L. Anand, Fracture of metallic glasses at notches: Effects of notch-root radius and the ratio of the elastic shear modulus

to the bulk modulus on toughness, Acta Mater. **57**, 6057 (2009).
197 C. H. Rycroft, and E. Bouchbinder, Fracture toughness of metallic glasses: Annealing-induced embrittlement, Phys. Rev. Lett. **109**, 194301 (2012).
198 B. Ding, X. Li, X. Zhang, H. Wu, Z. Xu, and H. Gao, Brittle versus ductile fracture mechanism transition in amorphous lithiated silicon: From intrinsic nanoscale cavitation to shear banding, Nano Energy **18**, 89 (2015).
199 J. R. Rice, and R. Thomson, Ductile versus brittle behaviour of crystals, Philos. Mag.-J. Theor. Exp. Appl. Phys. **29**, 73 (1974).
200 A. Kelly, W. R. Tyson, and A. H. Cottrell, Ductile and brittle crystals, Philos. Mag.-J. Theor. Exp. Appl. Phys. **15**, 567 (1967).
201 H. Gao, B. Ji, I. L. Jager, E. Arzt, and P. Fratzl, Materials become insensitive to flaws at nanoscale: Lessons from nature, Proc. Natl. Acad. Sci. USA **100**, 5597 (2003).
202 S. J. Poon, A. Zhu, and G. J. Shiflet, Poisson's ratio and intrinsic plasticity of metallic glasses, Appl. Phys. Lett. **92**, 261902 (2008).
203 A. C. Lund, and C. A. Schuh, Yield surface of a simulated metallic glass, Acta Mater. **51**, 5399 (2003).
204 A. C. Lund, and C. A. Schuh, The Mohr-Coulomb criterion from unit shear processes in metallic glass, Intermetallics **12**, 1159 (2004).
205 X. Lei, Y. Wei, B. Wei, and W. H. Wang, Spiral fracture in metallic glasses and its correlation with failure criterion, Acta Mater. **99**, 206 (2015).
206 R. T. Qu, Z. J. Zhang, P. Zhang, Z. Q. Liu, and Z. F. Zhang, Generalized energy failure criterion, Sci. Rep. **6**, 23359 (2016).
207 Z. Q. Song, E. Ma, and J. Xu, Failure of $Zr_{61}Ti_2Cu_{25}Al_{12}$ bulk metallic glass under torsional loading, Intermetallics **86**, 25 (2017).
208 B. Ding, and X. Li, An eccentric ellipse failure criterion for amorphous materials, J. Appl. Mech. **84**, 081005 (2017).

非晶合金失效行为与准则

陈艳, 戴兰宏

摘要 非晶合金具有优异的力学性能, 是一类新兴的先进结构材料. 然而, 该材料常温下表现的脆性断裂与复杂断裂行为极大地限制了其工程应用. 在过去的几十年, 国内外学者针对非晶合金的延性或脆性变形与断裂, 其中涉及材料成分、加载条件、样品尺寸等, 开展了广泛研究, 并在非晶合金失效行为认识上取得了重要进展. 剪切带、孔洞化和裂纹尖端场本质等微观断裂机制被一一揭示. 延脆转变行为与其内在的控制参数被发现. 为了有效描述和预测非晶合金的失效行为, 研究者们分别基于经验或从原子间相互作用出发, 建立了延性和脆性非晶合金的失效准则. 在本文中, 我们对以上进展进行了回顾和评述, 并提出了非晶合金失效有待进一步研究和厘清的重要问题.